

Two-compartment neuronal spiking model expressing brain-state specific apical-amplification, -isolation and -drive regimes

Elena Pastorelli¹, Alper Yegenoglu^{2,5}, Nicole Kolodziej^{1,3}, Willem Wybo⁴,
 Francesco Simula¹, Sandra Diaz², Johan Frederik Storm⁶, and Pier Stanislao Paolucci¹

¹Istituto Nazionale di Fisica Nucleare, Sezione di Roma, Roma, Italy

²Simulation and Data Lab Neuroscience, Jülich Supercomputing Centre (JSC), Institute for Advanced Simulation, JARA, Jülich Research Center, Jülich, Germany

³Dipartimento di Fisica, Università di Roma Sapienza, Roma, Italy

⁴Institute of Neuroscience and Medicine (INM-6) and Institute for Advanced Simulation (IAS-6) and JARA-Institute Brain Structure–Function Relationships (INM-10), Jülich Research Center, Jülich, Germany

⁵Department of Mathematics, Institute of Geometry and Applied Mathematics, RWTH Aachen University, Aachen, Germany

⁶Department of Molecular Medicine, Institute of Basic Medical Sciences, University of Oslo, Oslo, Norway

March 27, 2024

Abstract

Mounting experimental evidence suggests that brain-state-specific neural mechanisms, supported by connectomic architectures, play a crucial role in integrating past and contextual knowledge with the current, incoming flow of evidence (e.g., from sensory systems). These mechanisms operate across multiple spatial and temporal scales, necessitating dedicated support at the levels of individual neurons and synapses. A notable feature within the neocortex is the structure of large, deep pyramidal neurons, which exhibit a distinctive separation between an apical dendritic compartment and a basal dendritic/perisomatic compartment. This separation is characterized by distinct patterns of incoming connections and brain-state-specific activation mechanisms, namely, apical amplification, isolation, and drive, which are associated with wakefulness, deeper NREM sleep stages, and REM sleep, respectively. The cognitive roles of apical mechanisms have been demonstrated in behaving animals. In contrast, classical models of learning in spiking networks are based on single-compartment neurons, lacking the ability to describe the integration of apical and basal/somatic information. This work aims to provide the computational community with a two-compartment spiking neuron model that incorporates features essential for supporting brain-state-specific learning. This model includes a piece-wise linear transfer function (ThetaPlanes) at the highest abstraction level, making it suitable for use in large-scale bio-inspired artificial intelligence systems. A machine learning evolutionary algorithm, guided by a set of fitness functions, selected the parameters that define neurons expressing the desired apical mechanisms.

1 Introduction

Thanks to an evolutionary history spanning hundreds of millions of years and selecting from countless individuals, the structural connectome and cellular mechanisms have become adept at supporting the integration of multi-modal sensory evidence with internal hypotheses about the world and the self [39, 35, 53, 20]. Additionally, specialized solutions have emerged at the macro-, meso-, and micro-scales, enabling the expression of dynamic repertoires of functional connectivity [8]. At the cellular level, within large, cortical pyramidal cells of the mammalian neo-cortex, specific feed-forward sensory input is combined with contextual and feed-back information by the *apical-amplification* principle [41, 27, 30, 28], with [42] assuming apical mechanisms to be among key cellular foundations of the mental life. While this type of amplification seems to dominate during wakefulness [27], evidence suggests that it is replaced by different principles and mechanisms during transitions

to other brain-states [3, 2], namely *apical-isolation* during the deepest stages of NREM sleep (like in anesthesia [56]) and *apical-drive* during dreaming [3]).

The existence of different brain states, supported by state-specific cellular and systemic mechanisms, is also of ancient origin. Sleep has withstood the evolutionary pressure across all studied animal species, despite its apparent lack of productivity. It promotes memory consolidation and integration, as well as preparation for anticipated tasks [60, 7, 50], and returns the network to optimal working points after periods of awake learning [62, 59]. Mammals devote a significant portion of their time to sleep, especially youngsters who learn at the fastest rate [52]. Moreover, sleep deprivation negatively impacts cognitive performance [25]. These considerations underscore the importance of detailed modeling of sleep’s cognitive functions and the underlying cellular mechanisms.

Here, we propose a method to transition from the classical modeling approach of networks, which relies on single-compartment neurons, towards incorporating simple apical Ca^{2+} -dynamics. This inclusion supports the expression of intriguing brain-state-specific learning capabilities. Single-compartment models with spike frequency adaptation, such as the Adaptive Exponential Integrate and Fire neuron (AdEx) [6], have enabled the construction of networks capable of entering both wakefulness-like asynchronous irregular regimes and deep-sleep-like synchronous slow oscillation regimes (e.g., [40], [12]). For such networks, mean-field models have been developed [61]. These mean-field descriptions of the behavior of spiking networks composed of AdEx neurons have supported the development of models based on connectomes at the scale of the whole brain [61, 1], also capable of expressing both the asynchronous and synchronous regimes. However, these models do not capture the activity of individual neurons and synapses in engram coding, nor do they support the simulation of the temporal evolution of engrams [24].

The cognitive and energetic functions specific to different brain states have been explored in spiking models engaged in learning and sleep cycles. These models aim to simulate the activity and contribution of individual neurons and monitor synaptic changes over time [11, 19, 31]. Although these models utilize the temporal coincidence between contextual and perceptual information, they are still based on single-compartment neurons. Therefore, they necessitate precise calibration of currents carrying contextual priors and novel evidence. Such modeling approaches cannot fully leverage the capabilities of apical mechanisms, for example, the transition to much higher frequencies associated with *apical-amplification* during wakefulness, *apical-drive* during dreaming, or *apical-isolation* during deep, slow-wave sleep.

Within the framework of bio-inspired artificial intelligence, a few studies (e.g., [9, 10]) have begun to explore the specific advantages of apical-amplification-like bursting mechanisms for fast learning in spiking networks engaged in complex temporal tasks. However, these models have taken as working hypotheses the existence of transfer functions that enter a bursting regime when a temporal coincidence between perceptual and sensorial signals is detected. Here, we demonstrate how to construct a two-compartment neuron based on cellular biophysical evidence, capable of supporting the apical-amplification bursting mechanism. Furthermore, bio-inspired Artificial Intelligence (AI) algorithms would benefit from neural models characterized by a simple transfer function, simplifying the definition of training rules. A classic transfer function adopted in AI algorithms is the ReLU (rectified linear unit) rule, which approximates the transfer function of single-compartment neurons. We will show how to introduce a transfer function suitable for approximating the response of the two-compartment neuron to the combination (I_s, I_d) of somatic and distal signals, capable of describing the apical-amplification, -isolation, and -drive regimes. We have named this transfer function $\text{ThetaPlanes}(I_s, I_d)$.

The extension of the AdEx model to include an apical compartment with simplified Ca^{2+} -dynamics (the Ca-hotzone, here abbreviated to Ca-HZ) requires a few tens of parameters, implying a search in a high-dimensional space for fine-tuning. For any mathematical model, understanding the sensitivity of the model output to perturbations and correlations among the parameters defining it is crucial. This need becomes even more apparent when dealing with high-dimensional parameter spaces, where the dependency of outputs on underlying parameters becomes less intuitive for the modeler. As in many other research fields, neuroscience demands a thorough understanding of these relationships to draw meaningful conclusions about the simulated behavior of the modeled phenomena [37, 68]. Population-based optimization techniques offer a more efficient approach to exploring large parameter spaces than brute-force testing of all possible parameter combinations. Depending on the shape of the manifolds, different algorithms may be more or less effective in navigating the parameter space and identifying areas of interest to the modeler. While, for example, gradient-based methods typically identify local minima and converge very quickly, not all fitness evaluation measures and parameter spaces are suitable for such algorithms [67]. Simulated annealing and cross-entropy methods provide suitable gradient-free exploration techniques but

also require fine-tuning of hyperparameters. Evolutionary strategies and similar population-based methods can effectively navigate complex parameter spaces and quickly adapt to the manifolds if the level of noise or stochasticity is maintained at a suitable level, depending on the variations induced by the parameters with respect to the fitness. Several such algorithms can be tested and even combined to achieve a comprehensive understanding of parameter sensitivity and interdependencies. The tools and methodology adopted in this work to explore the parameter space defining the two-compartment model we named *Ca-AdEx*, and the evolutionary approach based on the definition of a *genome* and a *fitness function*, are detailed in dedicated subsections of *Methods*.

Multi-compartment (MC) models have been successful in reproducing experimentally observed dendritic processes and computations [49], particularly the interaction between apical Ca^{2+} -spikes and somatic action potentials [21]. Most often, MC models are paired with Hodgkin-Huxley (HH) type ion channels. The spatially extended nature of the dendritic tree, requiring many compartments, leads to models that are expensive to simulate. Past simplification efforts have focused on two largely orthogonal axes of advance: either condensing the HH channels into a simpler effective spike generation mechanism [26, 45] or reducing the number of compartments needed in a simulation while maintaining desired response properties [66]. To ultimately arrive at the most efficient formulation of a neuron model, a simplified description of dendritic non-linearities needs to be combined with a reduction in the number of compartments, in such a way that the model architecture is flexible and can admit a range of dendritic computations. Previous work on this topic used a hybrid combination of compartment dynamics and kernel convolutions [36], the former to model Ca^{2+} -activation and the latter to capture the somato-dendritic interactions. While the use of convolutions is a general way to capture the linear component of intra-dendritic interactions [64, 63], it is computationally inefficient compared to the use of normal coupling terms between compartments [66]. For this reason, we propose an approach that solely relies on normal compartmental dynamics, which has the added advantage of potentially integrating any type of nonlinear conductance. By design, this approach can thus also implement other dendritic non-linearities, such as N-Methyl-D-Aspartate (NMDA) spikes [48, 34, 33]. We demonstrate this potential by extending the two-compartment Ca-AdEx model to a multi-compartment description, which, next to the Ca-HZ and soma compartments, features apical and basal compartments suited for NMDA-spike generation. Furthermore, we have implemented a compartmental modeling framework in NEST [18, 54] that supports the aforementioned Ca^{2+} -, AdEx-, and NMDA dynamics. Combined, our work facilitates the study of dendritic dynamics with simplified neuron models at the network level.

2 Methods

2.1 The two-compartment Ca-AdEx model supporting calcium spike firing

One of the focal points of this endeavor was the creation of a neuron model able to express properties of apical amplification during awake states, to aid the formation of memories inside the synaptic matrix during incremental learning cycles. Indeed, recent studies ([2, 3]) have highlighted the critical role of apical amplification for conscious processing during the awake state in layer 5 pyramidal neurons (L5PC), in contrast with the mechanisms of apical drive and apical isolation that are predominant respectively in REM and NREM sleep. To replicate these states, it is essential to have an apical compartment able to support Ca^{2+} -spike, ([30, 27]), considered as the cellular mechanism underpinning apical amplification. Meanwhile, the soma follows the dynamics of an adaptive exponential integrate and fire neuron (AdEx), described by the following equations ([17]):

$$\begin{cases} C_m \frac{dV}{dt} &= -g_L(V - E_L) + g_L \Delta_T \exp\left(\frac{V - V_{th}}{\Delta_T}\right) - g_e(t)(V - E_e) - g_i(t)(V - E_i) - w + I_e \\ \tau_w \frac{dw}{dt} &= a(V - E_L) + b \sum_k \delta(t - t_k) - w \end{cases} \quad (1)$$

The parameters are detailed in the *Soma passive parameters* section of table 1, while I_e represents all the external currents.

The backpropagation-activated calcium spikes (BAC firing) is induced by the coincidental occurrence of a synaptic input to the apical dendrite and a spike generated within the soma. This spike backpropagates to the Ca-HZ within the apical dendrite (BAP), effectively lowering the threshold required for a dendritic Ca^{2+} -spike. Consequently, this mechanism can trigger a burst of multiple action potentials, even in the presence of a subthreshold distal excitatory postsynaptic signal.

The activation of the calcium spike in the dendrite is the critical element for the BAC firing. To support this activation, we modeled a neuron implementing a voltage dependent Ca^{2+} current and the Ca^{2+} concentration dynamics within the apical dendritic compartment (Ca-HZ). Additionally, along a Ca^{2+} -activated K current is included to re-polarize the dendritic membrane and terminate the Ca^{2+} -spike.

The dendritic intracellular Ca^{2+} concentration dynamics has been modeled, as described in [17], using the following equation:

$$\frac{d[Ca]}{dt} = \phi_{Ca} I_{Ca} + \frac{[Ca] - [Ca]_0}{\tau_{Ca}} \quad (2)$$

where $[Ca]_0$ represents the baseline of the intracellular Ca^{2+} concentration in mM, τ_{Ca} is the time constant of calcium extrusion in ms, I_{Ca} is the high voltage activated Ca^{2+} current circulating in the dendrite in pA and ϕ_{Ca} is a scaling factor.

The dendritic ion currents were modeled using the Hodgkin-Huxley formalism. The high voltage activated Ca^{2+} current (I_{Ca}) has been modeled as in [29]:

$$I_{Ca} = g_{Ca} m h (E_{Ca} - V) \quad (3)$$

where g_{Ca} is the maximal calcium conductance in nS, E_{Ca} is the calcium reversal potential and V the membrane voltage, both in mV. The activation and inactivation variables, m and h respectively, are characterized by first-order kinetics:

$$\frac{dm}{dt} = \frac{m_\infty - m}{\tau_m} \quad \text{and} \quad \frac{dh}{dt} = \frac{h_\infty - h}{\tau_h} \quad (4)$$

where m_∞ and h_∞ are the corresponding steady state functions and τ_m and τ_h are their time constants in ms. The steady state functions are given by:

$$m_\infty = \frac{1}{1 + \exp(m_{slope}(V - (m_{half})))} \quad \text{and} \quad h_\infty = \frac{1}{1 + \exp(h_{slope}(V - (h_{half})))} \quad (5)$$

with m_{slope} and h_{slope} representing the slope of the two functions and m_{half} and h_{half} representing the half activation/deactivation values in mV.

The Ca^{2+} activated K current ($I_{K_{Ca}}$) has been modeled as in [21]:

$$I_{K_{Ca}} = g_K m (E_K - V) \quad (6)$$

where g_K is the maximal potassium conductance in nS, E_K is the potassium reversal potential and V is the membrane voltage, both in mV. m represents the activation variable described by the first order kinetics:

$$\frac{dm}{dt} = \frac{m_\infty - m}{\tau_m} \quad (7)$$

Here τ_m is the potassium time constant in ms and m_∞ is the activation steady state variable described by:

$$m_\infty = \frac{1}{1 + \left(\frac{Ca_{th}}{[Ca]}\right)^{\exp_{K_{Ca}}}} \quad (8)$$

where Ca_{th} represents the Ca concentration threshold for calcium channel opening in mM and $\exp_{K_{Ca}}$ is an exponential factor.

In summary, a simple two-compartment Ca-AdEx neuron is described by equation (23) in Section 3.1.

The AdEx mechanism and Ca^{2+} currents were implemented within the NEST compartmental modelling framework (2.8), allowing their incorporation in the somatic and Ca-HZ compartment, respectively.

2.2 The *genome* of the Ca-AdEx model

The behaviour of a neuron model is characterized by a set of parameters required to describe its dynamics. In this paper we named this set of parameters as the *genome* of the neuron, because it has been identified using an evolutionary algorithm. For the multi-compartment neuron model, this genome comprises all parameters,

both passive and active, necessary to define the dynamics of each compartment and all the ionic currents involved.

The passive parameters which pertain to membrane properties, allow neurons to conduct electrical impulses without the use of voltage-gated ion channels. These parameters detail the membrane potential changes in response to currents across the cell membrane. Among the passive neuron parameters, we include the capacitances (C_m), leak conductances (g_L , i.e. conductances that do not vary with the membrane potential or other parameters), and reversal potentials of both somatic and dendritic compartments (E_L). These are responsible for the under-threshold and spike-triggered dynamics described in equation 1.

The parameters governing the ionic currents are defined as active parameters. In the model utilized in this work, the active parameters encompass all those used to describe the dynamics of calcium concentration, the voltage dependent calcium current and the calcium activated potassium current.

Table 1 presents the complete genome used to describe the Ca-AdEx neuron defined in this work.

Section 6 reports the genome of the best Ca-AdEx neuron identified by the evolutionary search, used in next sections, if not otherwise stated.

Table 1: Neuron Genome: parameters characterizing the Ca-AdEx neuron. See Section 6 for the values of the neuron identified by the evolutionary search.

Soma passive parameters		
C_m^s	Membrane capacitance	pF
g_L^s	Leakage conductance	nS
E_L^s	Leakage reversal potential	mV
t_{ref}	Refractory period	ms
Δ_T	Slope factor	mV
a	Subthreshold adaptation	nS
b	Spike-triggered adaptation	pA
τ_w	Adaptation time constant	ms
V_{th}	Membrane voltage threshold	mV
V_{reset}	Membrane voltage after-spike reset	mV
w_{BAP}	BAP amplitude	mV
d_{BAP}	BAP delay	ms
Distal passive parameters		
C_m^d	Membrane capacitance	pF
g_L^d	Leakage conductance	nS
g_C	Soma-distal coupling conductance	nS
E_L^d	Resting potential	mV
Distal active parameters		
\bar{g}_{Ca}	Max Ca conductance	nS
τ_{Ca}	Ca decay time constant	ms
τ_m	Ca activating function time constant	ms
τ_h	Ca deactivating function time constant	ms
m_{half}	Ca activating function half voltage	mV
h_{half}	Ca deactivating function half voltage	mV
m_{slope}	Ca activating function slope	-
h_{slope}	Ca deactivating function slope	-
$[Ca]_{th}$	Ca concentration threshold for Ca channel opening	mM
$[Ca]_0$	Baseline intra-cellular Ca concentration	mM
ϕ	Scaling factor in Ca concentration dynamics	-
$\bar{g}_{K_{Ca}}$	Maximal conductance of Ca dependent K current	nS
$\tau_{K_{Ca}}$	Activating function time constant of Ca dependent K current	ms
$exp_{K_{Ca}}$	Exponential factor in Ca dependent K current	-
E_K	K reversal potential	mV

2.3 Fitness functions

Specific fitness functions have been devised to constrain the model. These functions aim to guide the evolutionary search within parameter space toward optimal configurations, focusing on the identification of neurons that embody both the spiking frequency–stimuli relationships characteristic of apical mechanisms and a response to somatic-only stimulus that mirrors the behaviour of a single-compartment AdEx neuron.

In our work, the model’s fitness was assessed considering two different tasks: response to *pulse stimuli* of a few milliseconds in duration and response to *prolonged stimuli* lasting few seconds.

In the *pulse stimuli* task, the Ca-AdEx neuron model is designed to replicate the experiment proposed in [30], demonstrating the apical amplification effects through the activation of the BAC firing in response to short-duration currents. The goal is to emulate the observations reported in the four panels of figure 1 from the cited study. These panels depict the response to four combination of short duration inputs delivered to the apical and somatic compartment. Notably, the most interesting scenario involves injecting a threshold step current into the somatic compartment for $5ms$, accompanied by an under-threshold *beta* current in the distal compartment with a $5ms$ delay. The threshold somatic current’s amplitude is calibrated elicit a single spike in isolation. Conversely, the provision of the under-threshold distal current alone does not produce any spike. The essential behaviour to replicate is that the combination of these two currents can activate the BAC firing mechanism, leading to a high-frequency burst of three spikes (see Figure 6). To guide the model towards accurately responding to the four combination of short-duration pulses, four fitness functions are employed. These functions aim to generate the correct number of spikes in short-duration bursts and to delineate a regime of under-threshold distal stimulus (see the *Pulse stimuli* section of table 2).

In the second optimization task, the *prolonged stimuli* task, the neuron model is subjected to pairs of prolonged-duration (I_s, I_d) DC input currents. Combinations of somatic and distal stimuli are kept constant for $2s$, followed by a $3s$ period of zero input. The corresponding set of fitness functions is detailed in the *Prolonged stimuli* section of table 2. In this scenario, the computation of fitness functions relies on several different measures. Initially, evaluations are made concerning the activation of Ca^{2+} channels and, following activation, their closure after the stimulus concludes. Moreover, individuals (i.e., model configurations) that activate calcium spikes even with purely somatic currents are excluded by a dedicated fitness function.

Then, our goal is to develop a two-compartment neuron that, when stimulated somatically, mimics an equivalent single-compartment AdEx neuron. To achieve this, we defined two fitness functions. The first employs the Earth Mover’s Distance (EMD) algorithm. Additionally, we compare the rheobase of the single-compartment and two-compartment neurons (refer to the *AdEx matching* subsection of table 2).

An additional set of fitness functions aims to ensure the model exhibits a high, linear gain associated with the apical mechanism (refer to *Gain & linearity of apical mechanism* in table 2). Specifically, for the $\nu(I_s, I_d)$ transfer function, evaluations include: the firing rate following Ca^{2+} opening for a distal-only stimulus ($I_s = 0, I_d$), and the linearity in the firing rate increase linked to calcium channel activation for increasing somatic and distal currents. Moreover, particular fitness functions focus on ensuring the monotonicity of the $\nu(I_s, I_d = const)$ curves and the presence of the apical gain mechanism across the desired input domain: $I_s = 0, \dots, I_s^{Max}, I_d = 0, \dots, I_d^{Max}$.

A fitness function is dedicated to excluding neurons exhibiting ”epileptic” behavior when stimulated within the predefined range of currents (refer to the *Exclusion of pathological configurations* section in table 2). Furthermore, an additional set of *Cautionary checks* is introduced to further constrain the neurons. However, these additional constraints have likely been redundant in the context of our numerical experiments.

Table 2: Fitness functions

Pulse stimuli task	
<i>L2_PD</i>	Number of spikes for (th I_s, I_d under-th) [target=3]
<i>L2_PE</i>	Number of spikes for ($I_s = 0, I_d$ over-th) [target=2]
<i>L2_PG</i>	Diff. of spikes between (I_s, I_d under-th) and ($I_s = 0, I_d$ over-th) [target=1]
<i>L2_PR</i>	I_d over-threshold / I_d under-threshold ratio
Prolonged stimuli task	
<i>Primary checks of apical channels activation</i>	
<i>L2_CaO</i>	Missed Ca channel opening
<i>L2_CaC</i>	Missed closure of apical mechanism
<i>L2_CaO_soma</i>	Check for Ca NOT opening for $I_d = 0$
<i>AdEx matching</i>	
<i>L2_SEMD</i>	EMD between adex and soma curves, target = 0
<i>L2_SH</i>	Somatic rheobase, target is single-compartment AdEx threshold
<i>Gain & linearity of apical mechanism</i>	
<i>L2_120CaH</i>	Distal firing rate after Ca opening
<i>L2_NUMJUMPS</i>	Number of jumps in f/I curves
<i>L2_LinJump</i>	Linearity in Ca jump for growing (I_s, I_d) currents
<i>L2_MONOTON</i>	Monotonicity of the f/I curves
<i>Exclusion of pathological configurations</i>	
<i>L2_E</i>	Check for epileptic neuron
<i>Cautionary checks</i>	
<i>L2_MINV</i>	Minimum voltage, target is adex minimum voltage
<i>L2_CSG_R</i>	Gain in in f/I curves due to calcium spike
<i>L2_DS_R</i>	Ratio between somatic and distal thresholds, when distal firing rate $\dot{v} > 4\text{Hz}$
<i>L2_SHZD</i>	Ratio between somatic and distal thresholds

2.4 The Learning to Learn framework

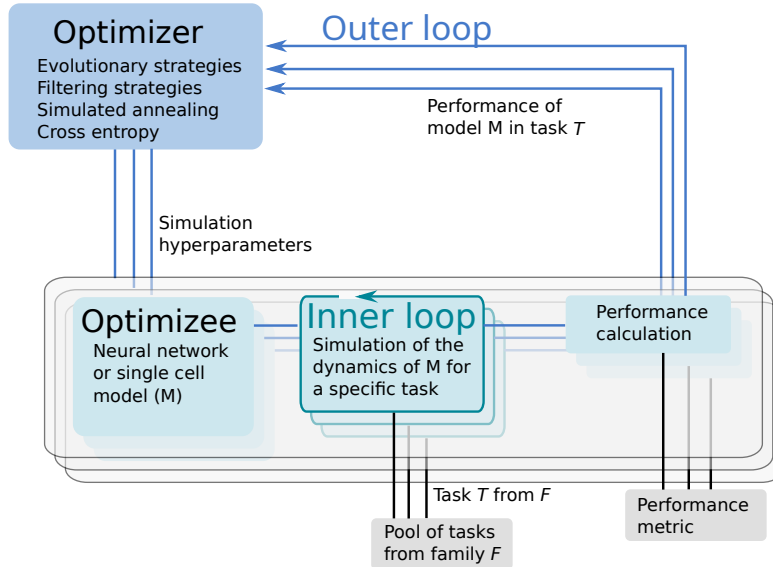


Figure 1: The two-loop scheme of L2L. In the inner loop, a model is trained or simulated on a task from a family of tasks. A fitness function evaluates the performance of the model. The model parameters are optimized in the outer loop. Image provided by [68].

Learning-to-learn, or meta-learning [57, 58], is an approach in machine learning aimed at enhancing learning performance through generalization. In a conventional learning setting, a program or algorithm is trained to perform a single task, evaluated by a specific performance metric. The algorithm’s performance improves as it is

exposed to more training samples. After sufficient training, the algorithm or model can achieve high performance on new samples of the same task that it did not encounter during the training phase.

In learning-to-learn, this paradigm is broadened into a two-loop structure, as shown in Figure 1. In the inner loop, the program, also known as the *optimizee*, can adapt to learn a specific task from a family of tasks. These tasks may range from classification and inference to training multi-agents for complex problem-solving. A fitness function assesses the performance of the optimizee and yields a fitness value. This function is tailor-made for the task and must be precisely defined to effectively evaluate the optimizee. In the outer loop, the algorithm’s overall performance is enhanced by optimizing the hyper-parameters or parameters across a spectrum of tasks, facilitating the evolution of the entire system.

In [68], we introduced an implementation of the learning-to-learn concept within a framework named *L2L*. In L2L, the outer loop is composed of various gradient-free optimization techniques based on metaheuristics, including evolutionary algorithms or filtering strategies. The framework’s versatility allows for the execution of any algorithm or simulation, which can then be operated on anything from local machines to high-performance computing systems (HPCs). Thanks to the framework’s inherently parallel structure, multiple instances of the inner loop can be efficiently deployed on HPC systems. L2L necessitates only a performance measure and a set of parameters for optimization targets. It is developed in Python, is available as open-source, and adheres to an open development model.

2.5 Execution Environment of L2L on HPC Platforms

L2L is equipped to iteratively deploy instances of the inner loop on HPC resources in a variety of ways. It is compatible with any scheduler present on a cluster or supercomputer. For this project, deployment occurred on the JUSUF supercomputer at the Jülich Supercomputing Center, as well as on the local cluster at the University of Rome. In both instances, slurm served as the scheduler to allocate the necessary computational resources.

In this work, for each optimization run we request a single allocation which comprises enough computational resources to launch all individuals in each iteration of the outer loop. Subsequently, L2L launches NS steps within the job allocation to distribute the resources among the individuals. This distribution is achieved by setting the appropriate scheduler parameters within the “exec” entry in the ‘JUBE_parameters” configuration. An example of such an entry is: `srun -N 1 -n 128 -c 1 --exact python`, where `srun` is the command to initiate a slurm step within an existing allocation, `-N` specifies the number of nodes, `-n` defines the number of MPI processes, `-c` denotes the number of cores per process assigned to this step, and `--exact` tells the scheduler to assign only the previously specified resources to this slurm step. This configuration is detailed within the L2L execution script.

2.6 Fitting the transfer function

Figure 2.a illustrates $\nu(I_s, I_d)$, the firing rate of the exemplary two-compartment Ca-AdEx neuron identified by the evolutionary search algorithm (see Section 6 for its parameters) in response to various combinations of constant somatic and distal currents. The regularity observed in the contour lines of equal firing rate suggests the potential for simplified approximate representations of the transfer function. This section outlines the method employed to derive such an approximation. Two distinct regions of low and high firing rate are discernible in Figure 2.a, seemingly demarcated by a straight line. Hereafter, we use the index $i \in \{-, +\}$ to denote the regions of lower or higher firing rates, respectively. In the $+$ region, contour levels of equal firing rate appear to be linear, parallel, and evenly spaced, indicating that the transfer function could be approximated by a plane. For each (I_s, I_d) pair, the simulation identifies the activation of the High Voltage dependent Ca^{2+} channel, resulting in a Boolean mask $M_+(I_s, I_d)$ that delineates the activation region associated with high firing rates (refer to Figure 2.b).

Fitting planes ν_+ are defined by

$$\nu_+(I_s, I_d) = a_+ I_s + b_+ I_d + d_+ \tag{9}$$

and their parameters (a_+, b_+, d_+) have been identified in this work using the *LinearRegression* class from the *sklearn.linear_model* Python module (release 1.0.2). The same procedure returns the plane fitting the region of low activity M_- (i.e., the lower part of Figure 2.a), where the contour lines are also approximately linear and evenly spaced for firing rates above a threshold ν_{low} .

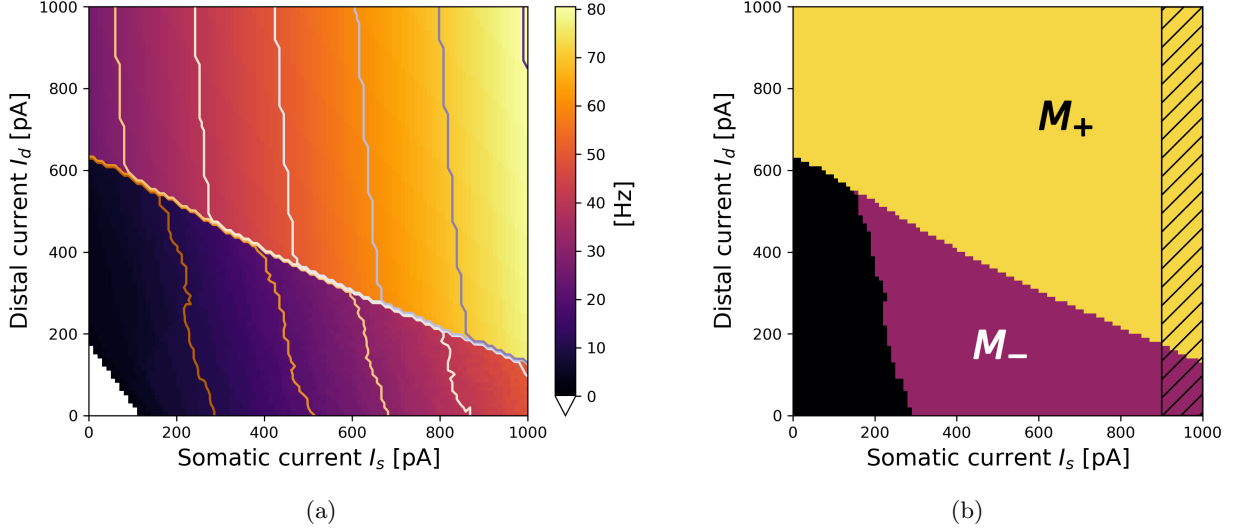


Figure 2: Search for approximating planes. a) Representation of $\nu(I_s, I_d)$, the firing rate of the two-compartment Ca-AdEx spiking neuron in response to combinations of somatic (I_s) and distal (I_d) currents. b) Algorithmic identification of M_+ and M_- regions from spiking simulation results.

The selection of an appropriate ν_{low} frequency is motivated by the need to model the learning advantages associated with apical amplification mechanisms, particularly in scenarios where external stimuli change at a fast rate. For instance, in a typical real-world scenario, sustaining a video rate of more than $20 frames/s$ is necessary, corresponding to an exposure to a stable perception lasting less than $50ms$. $\tau_{STDP} = 20ms$ is a commonly chosen duration for an STDP mechanism that captures either correlations (multiplicative STDP) or causal influence (additive STDP) between a presynaptic neuron (*pre*) and a postsynaptic neuron (*post*), with the pair of nearest spikes occurring at t_{post} and t_{pre} . Capturing even a single STDP-induced synaptic modification requires a minimum firing rate of $\nu_{low} > 10Hz$ and an exposure duration greater than $\simeq 50ms$. In this context, a single synaptic modification event would typically be induced with $t_{post} - t_{pre} > 2.5 \cdot \tau_{STDP}$. Therefore, for neurons capable of reaching significantly higher firing rates, capturing the regime of lower firing rates with extreme precision is not critical.

The $M_-(I_s, I_d)$ Boolean mask is defined by the points where the simulation indicates that $M_+(I_s, I_d) == false$ AND $\nu(I_s, I_d) > \nu_{low}$. The search for fitting planes can be done in the M_- region, employing the same algorithm used for M_+ , producing a $\nu_-(I_s, I_d)$ approximating plane.

To mitigate potential non-linearity at the boundaries of the region of interest, the Boolean masks excludes the region $I_s > I_{th}$, (illustrated as a dashed band in Figure 2.b). Figure 3.a and 3.b show the error (in Hz) between the planar fits $\nu_{-,+}(I_s, I_d)$ and the simulated transfer functions $\nu(I_s, I_d)$. The discrepancy between the firing rates obtained from simulation of the two-compartment Ca-AdEx neuron and those predicted by the fitting plane is discretised into $0.5Hz$ intervals, reflecting that firing rates are measured over simulation periods lasting two seconds.

The construction of $\nu_F(I_s, I_d)$, the simplified description over the entire range of I_s, I_d currents of the ν produced by spiking simulations, requires also a proper definition of the curve $I_d^H(I_s)$ that separates the M_+ from the M_- regions. $I_d^H(I_s)$ is the amount of distal current required to trigger a high firing regime (*H*) given a fixed value of somatic I_s current.

Figure 4 illustrates that the linear fit of the data representing the boundary between M_+ and M_- leads to the definition of the parameters θ_m^H , the slope of the fitting line, and θ_q^H , its offset. The resulting approximating line is expressed as:

$$I_{d,F}^H(I_s) = \theta_m^H I_s + \theta_q^H \quad (10)$$

Finally, the rheobase of the fitting function is defined by the combinations of currents that satisfy the condition $\nu_-(I_s, I_d) = 0$, this results in the line:

$$I_{d,F}^\rho(I_s) = \theta_m^\rho I_s + \theta_q^\rho \quad (11)$$

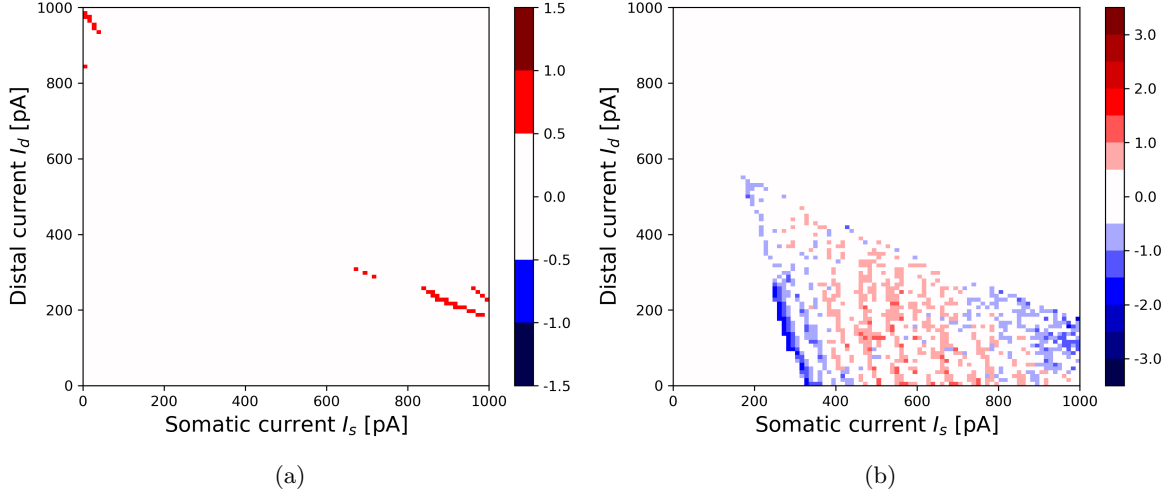


Figure 3: Errors of fitting planes (Hz). Panel a) M_+ region: $\nu_+ - \nu$. b) M_- region: $\nu_- - \nu$.

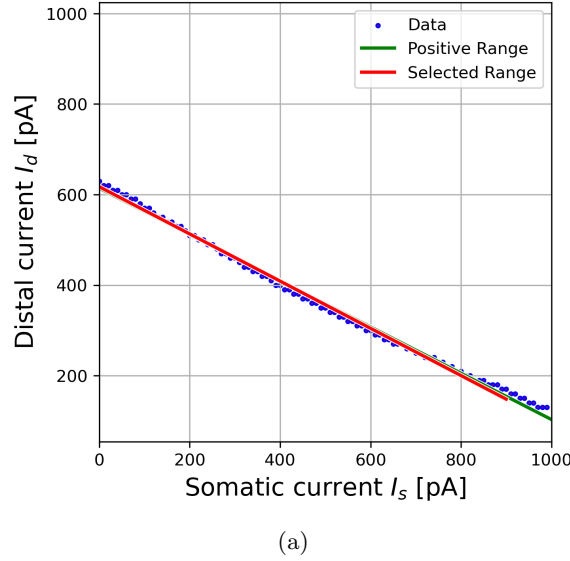


Figure 4: Linearity of the separation between the high activity M_+ region and the lower activity M_- region. (red line): $I_{d,F}^H(I_s)$ linear fit.

In summary, three planes ($\nu_0 = 0$, $\nu_-(I_s, I_d)$ and $\nu_+(I_s, I_d)$) are identified by the algorithm to approximate the activity in each region. The active approximated domain is limited/bounded by:

$$\Theta_H(I_s, I_d) = \Theta(I_d - I_{d,F}^H(I_s)) \quad (12)$$

The passive approximated domain is given by the product of two Θ s, namely:

$$\Theta_\rho(I_s, I_d) = \Theta(I_d - I_{d,F}^\rho(I_s)) \quad (13)$$

and

$$\Theta(-I_d + I_{d,F}(I_s)) = (1 - \Theta_H(I_s, I_d)) \quad (14)$$

Finally, the fitting function that spans the entire domain, as determined by the algorithm, is:

$$\nu_F(I_s, I_d; \nu) = \Theta_\rho(1 - \Theta_H) \cdot \nu_- + \Theta_H \cdot \nu_+ \quad (15)$$

This is referred to as *ThetaPlanes* in the following.

Table 3: Parameters of the *ThetaPlanes* piece-wise linear approximating function. See Section 6 for representative values.

ν_+ plane, apical amplification region	
a_+	Hz/pA
b_+	Hz/pA
d_+	Hz/pA
ν_- plane, lower firing rate region	
a_-	Hz/pA
b_-	Hz/pA
d_-	Hz/pA
$I_{d,F}^H(I_s)$, line of separation between regions	
θ_m^H	-
θ_q^H	pA
$I_{d,F}^P(I_s)$, rheobase line	
θ_m^P	-
θ_q^P	pA

2.7 Modulating the apical-amplification, -isolation and -drive regimes

A few parameters serve as simulation proxies for the effects of neuromodulation, facilitating transitions to apical-isolation-like and apical-drive-like regimes or modulating the apical-amplification behavior. [2] offers conceptual guidelines that have inspired the approach described here. As a proxy for ACh modulation, we consider the Spike Frequency Adaptation coefficient b in eq.1. Changes in excitability, associated with the level of NA, can be induced by, for example, altering the leakage reversal potential of the compartments ([16]). Additionally, exploring the effect of a change in the conductance that connects the two compartments is of interest. Figure 5 reports the results of the exploration in terms of neuromodulation for different brain states, using the parameters described in Table 4.

Table 4: Parameters to modulate the apical-amplification, -isolation, and -drive regimes. The apical-amplification configuration named a is the one identified by the evolutionary search (see Section 6 for its complete genome.)

Apical-amplification					Apical-isolation					Apical-drive				
Panel	b	g_C	E_L^d	E_L^s	Panel	b	g_C	E_L^d	E_L^s	Panel	b	g_C	E_L^d	E_L^s
a	40	1	-53	-63	d	200	1	-58	-68	g	0	1	-53	-68
b	50	1	-53	-63	e	200	0.3	-58	-68	h	20	1	-53	-68
c	60	1	-53	-63	f	200	0	-58	-68	i	40	1	-53	-68

2.8 Support for multi-compartment neurons in NEST

To leverage existing technology for the efficient simulation of recurrently connected spiking neural networks, we have integrated a general multi-compartment (MC) modeling framework into NEST. Generally, MC models can be represented as

$$C^i \frac{dV^i}{dt} = g_L^i (E_L^i - V^i) + \sum_{c \in \mathcal{C}^i} I_c^i(\mathbf{y}_c^i, V^i) + \sum_{r \in \mathcal{R}^i} I_r^i(\mathbf{y}_r^i, V^i, S_r^i) + \sum_{j \in \mathcal{N}^i} g_C^{ij} (V^j - V^i), \quad (16)$$

where V^i denotes the membrane potential in compartment i , C^i its capacitance, g_L^i its leak conductance and E_L^i the leak reversal potential. An arbitrary set \mathcal{C}^i of ion channels may be present in compartment i . Their current $I_c^i(\mathbf{y}_c^i, V^i)$ depends on the local membrane potential and a set of channel state variables \mathbf{y}_c^i . Similarly, an arbitrary set \mathcal{R}^i of synaptic receptors can exist, whose current may depend on state variables \mathbf{y}_r^i , the membrane potential, and the presynaptic input spike train S_r^i . Finally, the compartment i is coupled to its neighbours \mathcal{N}^i through a coupling conductance g_C^{ij} . Due to the conservation of current, the coupling is symmetric, i.e. $g_C^{ij} = g_C^{ji}$. By identifying the compartments with the nodes of a graph and the neighbour couplings with the edges, the MC model is always a tree graph.

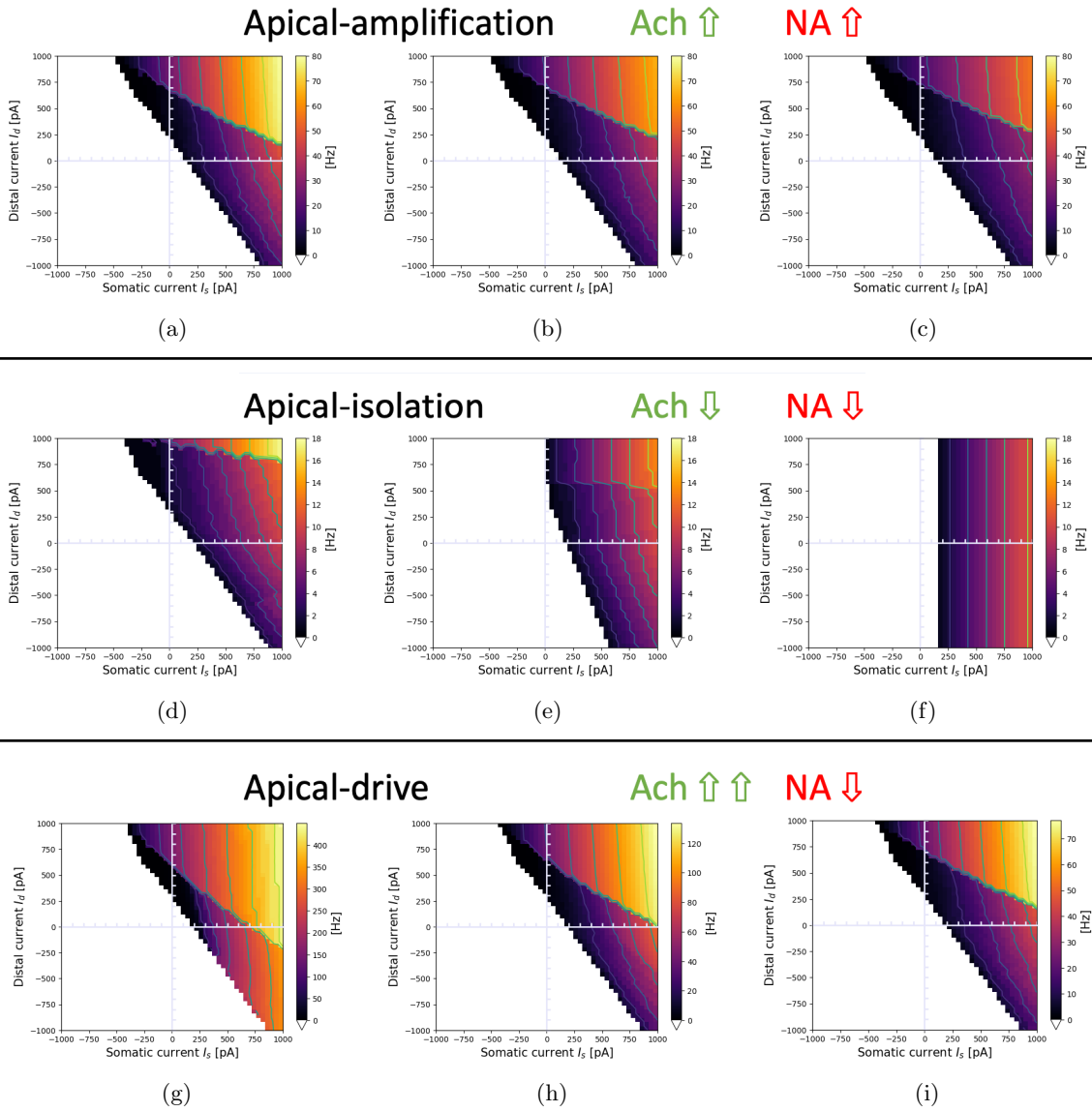


Figure 5: Proxies for ACh and NA modulation. Inducing a range of apical-amplification -isolation and -drive like configurations from the same starting neuron. Parameters in table 4

In simulation tools for detailed biophysical models, the continuous cable model of neuronal morphology is discretized spatially through the second-order finite difference approximation [14], and the resulting system of equations takes the form of (16). The number of compartments, or inversely their separation, is often chosen based on the electrotonic length constant. At a more abstract level, simplified multi-compartment (MC) models with two or three compartments are frequently utilized to represent elementary aspects of dendritic computation, with the parameters of (16) being tuned by ad-hoc methods for the specific scientific problem under investigation [43, 15, 36]. Between these levels of detail, compartmental parameters can be derived from full morphologies through matrix algebra to simulate local computations [66], or they can be explicitly tuned to replicate these computations [38].

The compartmental model architecture in NEST accommodates all these use cases by offering API functionality that enables end users to directly set compartmental parameters and arrange them in a user-specified tree graph layout. Furthermore, it is designed to be straightforwardly extendable with ion channels and receptor currents at the C++ level.

The system is discretised in time using the Crank-Nicolson scheme:

$$C^i \frac{V^i(t+h) - V^i(t)}{h} = \frac{F^i(V^i(t)) + F^i(V^i(t+h))}{2}, \quad (17)$$

where F^i represents right-hand side of (16). It is important to note that this method is implicit in the voltage: $F^i(V^i(t+h))$ needs to be Taylor-expanded so that all terms containing $V^i(t+h)$ ($\forall i \in \text{MC}$) can be moved to the left-hand side. The resulting matrix equation is then solved efficiently through the Hines algorithm [22]. For the state variables of ion channels and receptor currents, we use the widely used leap-frog scheme: a state variable y is computed at $t + \frac{h}{2}$, and thus has this value in both $F^i(V^i(t))$ and $F^i(V^i(t+h))$. Conversely, to compute the time evolution of a state variables from $t + \frac{h}{2}$ to $t + \frac{3h}{2}$, the voltage $V^i(t+h)$ is taken to be constant over this time-step.

If the state variable follows the general Hodgkin-Huxley formalism, i.e.

$$\frac{dy}{dt} = \frac{y_\infty(V) - y}{\tau_y(V)}, \quad (18)$$

the value at time $t + \frac{3h}{2}$ follows from integrating this equation as an initial value problem starting from $y(t + \frac{h}{2})$, which has the analytical solution:

$$y(t + \frac{3h}{2}) = P y(t + \frac{h}{2}) + (1 - P) y_\infty(V(t+h)),$$

with

$$P = \exp\left(-\frac{h}{\tau_y(V(t+h))}\right). \quad (19)$$

For state variables that do not depend on the voltage, as is often the case for those governing the synaptic conductance after spike arrival, efficiency is enhanced by precomputing the propagator P .

2.9 Detailed morphological neuron model

To demonstrate the potential of the MC modeling framework, we integrated Ca-AdEx into a neuron model that also includes dendritic compartments with NMDA-driven non-linearities, based after an L5PC morphology. This morphology was taken from Hay et al. [21] and implemented in NEAT [66]. We focused on the most important somatic Na^+ and K^+ channels (NaTa and Kv3.1) and opted for a passive dendritic membrane. The physiological parameters recommended by Major et al. [34] were adopted to replicate the amplitudes of glutamate-uncaging evoked NMDA-spikes in L5PC dendrites and somata, combined with a spine correction as in Rhodes et al. [46]. Concretely, this meant a specific capacitance of $0.8 \mu\text{F}/\text{cm}^2$, which was increased by a factor 1.92 to account for spine surface in dendrites with a radius smaller than $.6 \mu\text{m}$. The axial resistance was set at $100 \Omega \times \text{cm}$ for smooth dendrites, and $120 \Omega \times \text{cm}$ for spiny dendrites, while the specific membrane conductance was $100 \mu\text{S}/\text{cm}^2$, and the leak reversal was fixed at -75mV .

This model was then simplified into a description with six distal apical and 8 distal basal compartments that received AMPA+NMDA as well as GABA synapses, in addition to the soma and a Ca-hotzone compartment located where the main apical trunk splits into multiple branches. For technical reasons, all bifurcation sites in between any of those compartments are added automatically by the simplification procedure (Figure 9B, [66]). The parameters of the reduced model that also featured in the Ca-AdEx optimization procedure (such as the leak and capacitance of soma and Ca-HZ compartments, as well as their coupling) were overwritten by those obtained through the optimization, and the other optimized parameters of the Ca- and AdEx-mechanisms were added as well.

The resulting model was then stimulated with input current steps (Figure 9C), the BAC-firing protocol (Figure 9D) and Poisson distributed synaptic inputs (Figure 9E, F). For the BAC-firing protocol, we used a somatic current step amplitude of 750pA and a double exponential input current at the Ca-HZ compartment with $\tau_r = 1 \text{ms}$ and $\tau_d = 10 \text{ms}$, and which further had a maximal amplitude of 1500pA . For the Poisson synaptic inputs, AMPA and GABA receptors were simulated as the product of a double exponential conductance window [47] g and a driving force:

$$i_{\text{syn}} = g(e_r - v), \quad \text{with} \quad g = w n(\tau_r, \tau_d) \left(e^{-t/\tau_d} - e^{-t/\tau_r} \right). \quad (20)$$

Here, e_r is the synaptic reversal potential, τ_r and τ_d are the synaptic rise and decay time constants, and n a normalization constant that depends on τ_r and τ_d and normalizes conductance window g , so that its peak value is equal to the synaptic weight w . AMPA rise and decay times were $\tau_r = 0.2$ ms, $\tau_d = 3$ ms and AMPA reversal potential was $e_r = 0$ mV, whereas for GABA, we had $\tau_r = 0.2$ ms, $\tau_d = 10$ ms and $e_r = -80$ mV. NMDA currents [23] were implemented as:

$$i_{\text{syn}} = g \sigma(v) (e_r - v) \quad (21)$$

with $\tau_r = 0.2$ ms, $\tau_d = 43$ ms, and $e_r = 0$ mV, while $\sigma(v)$ – the channel’s magnesium block – had the form [4]:

$$\sigma(v) = \frac{1}{1 + 0.3 e^{-0.1 v}}. \quad (22)$$

The synaptic weight (i.e. maximum value of the conductance window) for the AMPA component of AMPA + NMDA synapses was set at 1 nS, and the maximal value of the NMDA window was twice that of the AMPA window (NMDA ratio of 2). GABA synapses also had a weight of 1 nS. While for the AMPA+NMDA synapses a multitude of Poisson input rates were probed as part of the scan (Figure 9F), the Poisson input rate to the GABA synapses was fixed at 20 Hz.

3 Results

3.1 Dynamics of the two-compartment Ca-AdEx neuron

By combining the multi-compartment neuron equation (16) with the AdEx equations (1), considering the ion currents detailed in equations (3) and (6), the calcium concentration dynamics (2), and the BAP contribution, the dynamics of Ca-AdEx neuron (outside the refractory period) is described by:

$$\left\{ \begin{array}{l} C_m^s \frac{dV^s}{dt} = -g_L^s (V^s - E_L^s) + g_L^s \Delta_T \exp\left(\frac{V^s - V_{th}^s}{\Delta_T}\right) + \\ \quad -g_e^s(t)(V^s - E_e^s) - g_i^s(t)(V^s - E_i^s) + \\ \quad -w + I_e^s - g_C(V^s - V^d) \\ \tau_w \frac{dw}{dt} = a(V^s - E_L^s) + b \sum_k \delta(t - t_k) - w \\ C_m^d \frac{dV^d}{dt} = -g_L^d (V^d - E_L^d) - g_e^d(t)(V^d - E_e^d) - g_i^d(t)(V^d - E_i^d) + \\ \quad + I_{Ca} + I_{K_{Ca}} + w_{BAP} \sum_k \delta(t - (t_k + d_{BAP})) + \\ \quad + I_e^d + g_C(V^d - V^s) \end{array} \right. \quad (23)$$

A somatic spike event is triggered when $V^s \geq V_{th}$, which defines the t_k spike time. V^s is set to the constant value V_{reset} during $t_k < t < t_k + t_{ref}$, while the distal compartment continues to integrate the dynamics defined by equation (23) during this period.

3.2 Response to pulse stimuli

Employing the L2L optimization framework to select neurons that best match our criteria led to the identification of the best fitting model. Figure 6 illustrates the behavior of the fitted model in response to input currents of short duration (a few milliseconds), according to the protocol for the *pulse stimuli* task outlined in 2.3. An under-threshold distal input, modeled as a beta function to mimic an excitatory postsynaptic potential (EPSP), slightly deflects the somatic membrane potential but does not trigger any spikes (6.a). A threshold somatic signal that evokes an action potential (AP) back-propagates through the axon, stimulating a Ca^{2+} influx that results in an increase in the distal membrane potential but is insufficient to initiate a calcium spike (6.b).

The concurrent application of the previous two input signals triggers a burst of two to three spikes at approximately 5 – 10Hz: the back-propagating action potential, induced by the threshold somatic input, lowers the membrane potential in the Ca-HZ. When coupled with the under-threshold distal input, this facilitates the

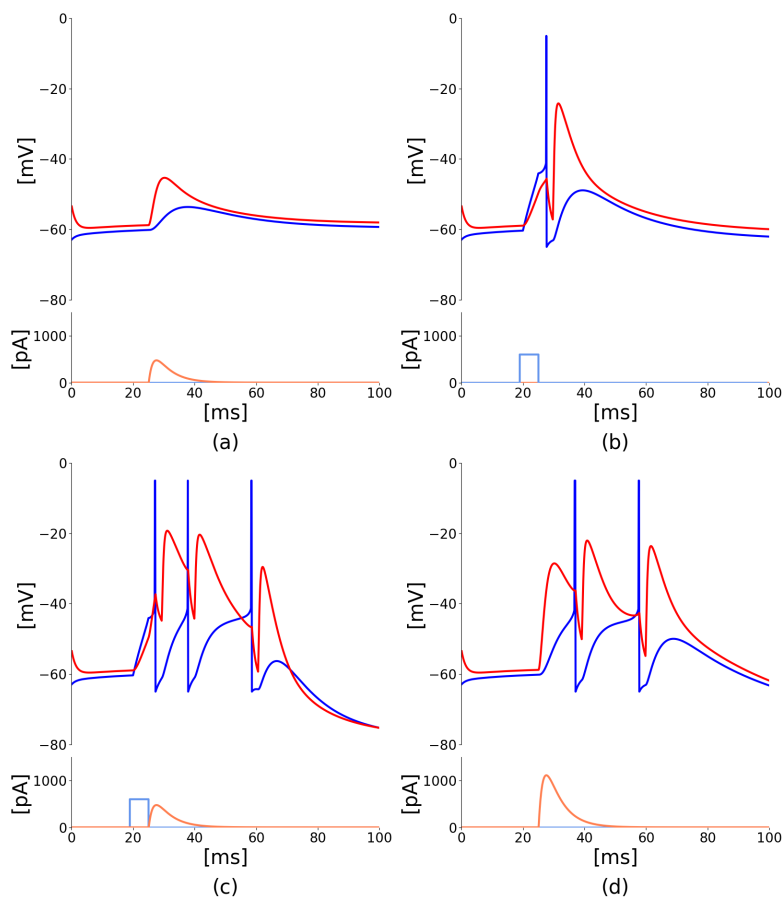


Figure 6: Response to pulse stimuli. (a) a beta-shaped current injection of 950pA (peak amplitude) at the distal compartment produces a deflection of only 11mV at the soma without eliciting any spike; (b) a threshold current injection (550pA) at the soma evokes one single AP; (c) the combination of a threshold somatic current as in b) and an under-threshold distal current as in a), separated by an interval of 5ms, activates the BAC firing mechanism and evokes a burst of three APs; (d) to obtain a burst using only distal injection, a current of at least 1350pA is required. All panels share scale bars and legend: in blue somatic membrane voltage; in red distal membrane voltage; in lightblue step somatic input; in orange beta-shaped distal input).

initiation of the calcium spike (6.c). To generate a similar burst with solely distal input, a higher peak current value must be supplied, as demonstrated in the example of 6.d. When combining somatic and distal input currents, the distal current is introduced with a delay of 5ms relative to the somatic one. Analyzing the neuron’s performance concerning this delay is not covered in this work, but it will be considered for further optimization of the neuron.

3.3 Response to prolonged stimulus: compact geometric description of the transfer function

Figure 7 summarizes the primary characteristics of the selected neuron in response to the *prolonged stimuli* task. Panel (a) illustrates the neuron’s dynamics for specific distal and somatic input currents, as administered according to the guidelines detailed in section 2.3. The orange line depicts the firing rate when the neuron is stimulated solely with a distal current. The activation of the BAC firing mechanism is indicated by the sharp increase in the firing rate observed at 630pA in the orange line: beyond this threshold, even without somatic input, a dendritic calcium spike is initiated, and the neuron enters into the active regime, wherein the mechanism of apical amplification becomes apparent. The other curves illustrate the neuron’s response when stimulated with a combination of currents injected into both the soma and the distal compartment. The visible jump in these curves corresponds to the neuron entering the active regime, a state reached when the combined effect of the two input currents is sufficient to trigger the calcium spike. As the value of the constant distal current increases,

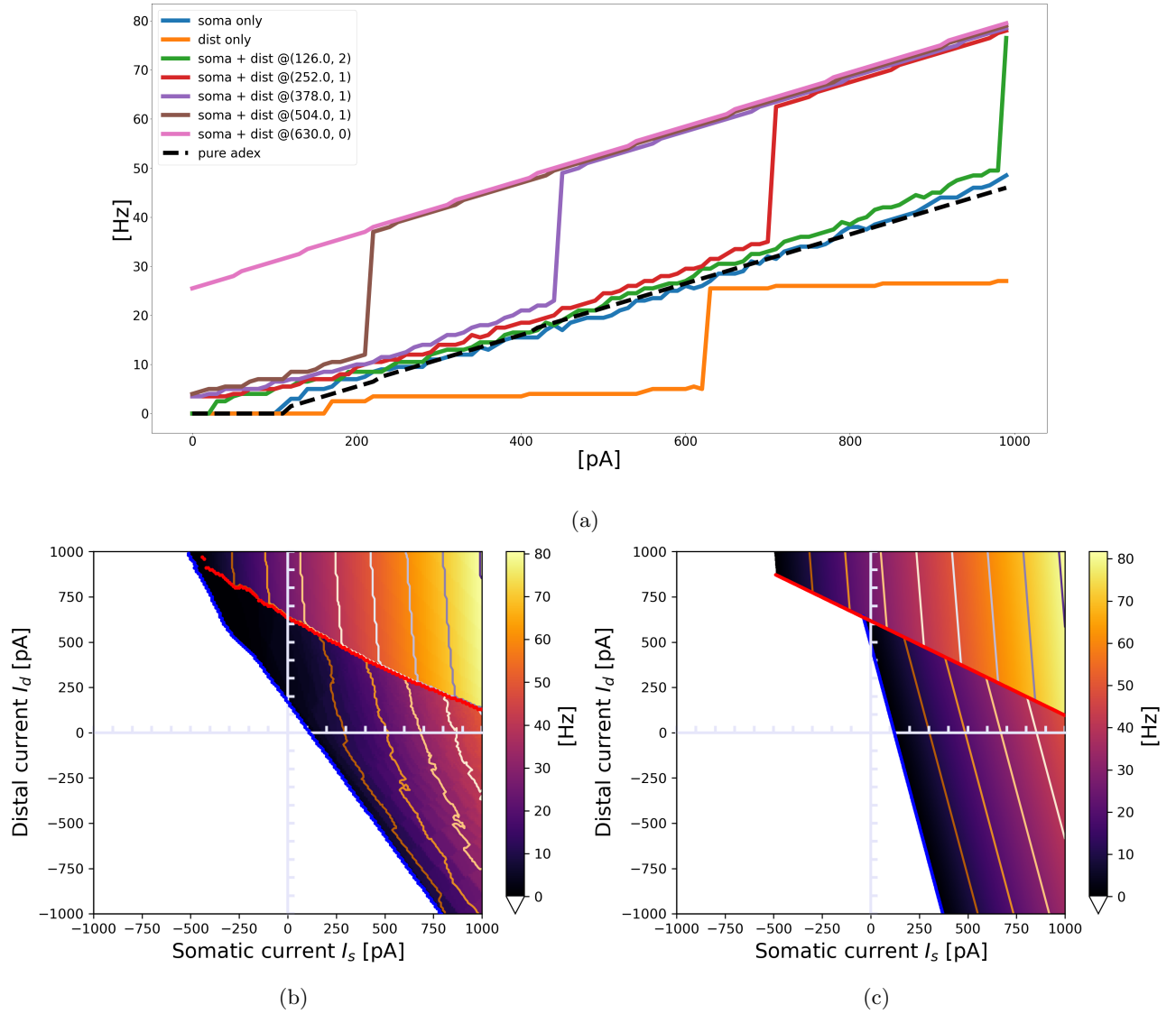


Figure 7: Transfer function of selected neuron and it's approximation with ThetaPlanes. (a) current to rate response to DC inputs delivered to different compartments: pure somatic current (blue), pure distal current (orange), combination of somatic and distal current (other colored lines). The dashed black line represents the transfer function of the AdEx neuron used as the target reference for the fitness function. (b) Transfer function of the neuron in the 2-D plane defined by somatic and distal input DC currents; in blue the rheobase and in red the transition line between passive and active calcium regimes, respectively expressing a lower and an higher firing rate. (c) ThetaPlanes approximating the transfer function.

the transition to the active regime occurs at progressively lower somatic input currents. The blue line represents the scenario where $I_d = 0$: neither the calcium spike nor the BAC firing mechanism is triggered, and within the analyzed range, the neuron behaves similarly to the pure AdEx model against which the two-compartment model has been fitted (indicated by the black dashed line).

Figure 7.b displays the firing rate of the neuron when stimulated with combinations of somatic and distal currents ($\nu(I_s, I_d)$). Three distinct regions are identifiable: the area below the blue line, where the firing rate equals 0 for every input current combination; an area of low firing rates situated between the blue and red lines; and an area of high firing rates above the red line, indicating the triggering of the calcium spike and the activation of the apical amplification mechanism (active regime). The blue line denotes the neuron's rheobase, while the

red line signifies the transition from the passive to the active regime. As discussed in the [Methods](#) section, by examining the firing rate ν of the multi-compartment neuron in the plane of input somatic and distal currents I_s and I_d , we can create a simplified model at a significantly higher level of abstraction. This is achieved through the definition of fitting planes: one for the apical amplification zone and another for the lower activity region of the neuron’s transfer function.

ν can be piece-wise by planes separated by lines, resulting in the *ThetaPlanes* transfer function:

$$ThetaPlanes(I_s, I_d; \nu) = \Theta_p(1 - \Theta_H) \cdot \nu_- + \Theta_H \cdot \nu_+ \quad (24)$$

Figure 7.c displays such approximating function.

Table 3 lists the parameters that define the *ThetaPlanes* function: the $\nu_-(I_s, I_d)$ and $\nu_+(I_s, I_d)$ planes, the transition line to high firing rates, and the rheobase. The *ThetaPlanes* configuration fitting the exemplary neuron is detailed in Section 6.

3.4 Wakefulness, NREM and REM specific apical mechanisms

Figure 8 illustrates the modulation of simulation proxies for ACh and NA to alter the transfer function of the exemplary two-compartment neuron discussed throughout this paper. Specifically, 8.a depicts a representative awake apical-amplification configuration; 8.b presents a configuration tailored to simulate the NREM sleep apical-isolation regime, and 8.c showcases a setting related to the apical-drive configuration, which is expected to be associated with a REM sleep regime.

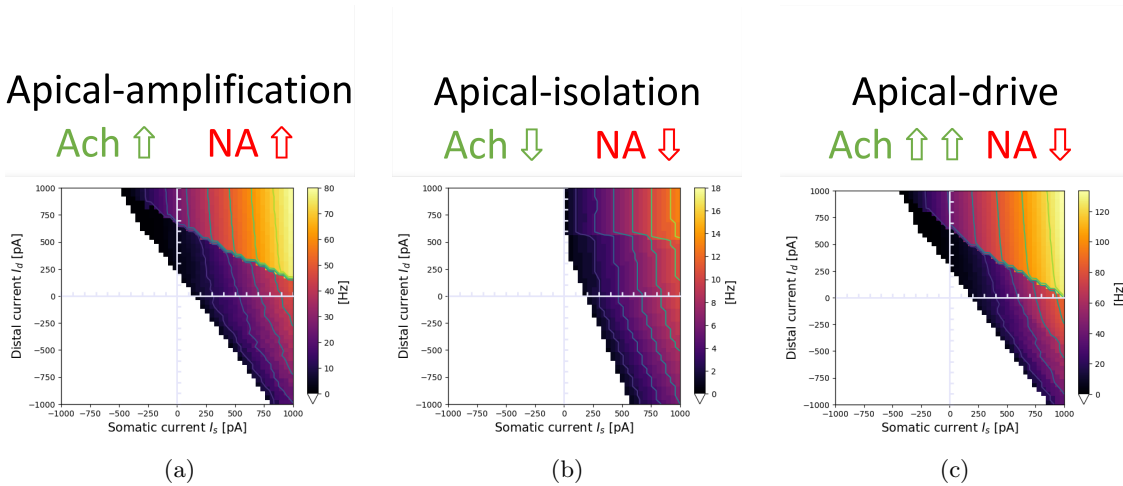


Figure 8: Apical-amplification, -isolation and -drive: exemplary $\nu(I_s, I_d)$ firing rates produced in the three regimes. Note: max ν is very different in the tree regimes: over 100Hz in apical-drive, up to 80Hz in -amplification and about 12Hz in -isolation. Also, the jump between the high-firing rate M_+ and the M_- regions spans from tens of Hz in the apical-drive regime down to a few Hz in the -isolation regime. (a) Apical amplification: $b = 40$, $g_C = 1$, $E_L^d = -53$, $E_L^s = -63$. (b) Apical isolation: $b = 200$, $g_C = 0.3$, $E_L^d = -58$, $E_L^s = -68$. (c) Apical-drive: $b = 20$, $g_C = 1$, $E_L^d = -53$, $E_L^s = -68$.

3.5 Extending the two-compartment layout

While important, the Ca^{2+} -spike is not the only dendritic event that fundamentally shapes the neuronal input/output relation (Figure 9A). Through the voltage dependent unblocking of the NMDA-receptor channel [32, 23], coincident inputs to dendritic branches summate supra-linearly, and the resulting events are known as NMDA-spikes [48, 34, 33]. As our Ca-AdEx framework is embedded in a general compartmental modelling framework, it is straightforwardly possible to extend the two-compartment description to one where there are additional dendritic subunits that can produce NMDA-spikes. We demonstrate the potential of our approach by deriving the parameters of these subunits from a realistic L5PC morphology (Figure 9B, [21]), using the method based on resistance matrix fits proposed by Wybo et al. [66]. The somatic and Ca-HZ compartment are then

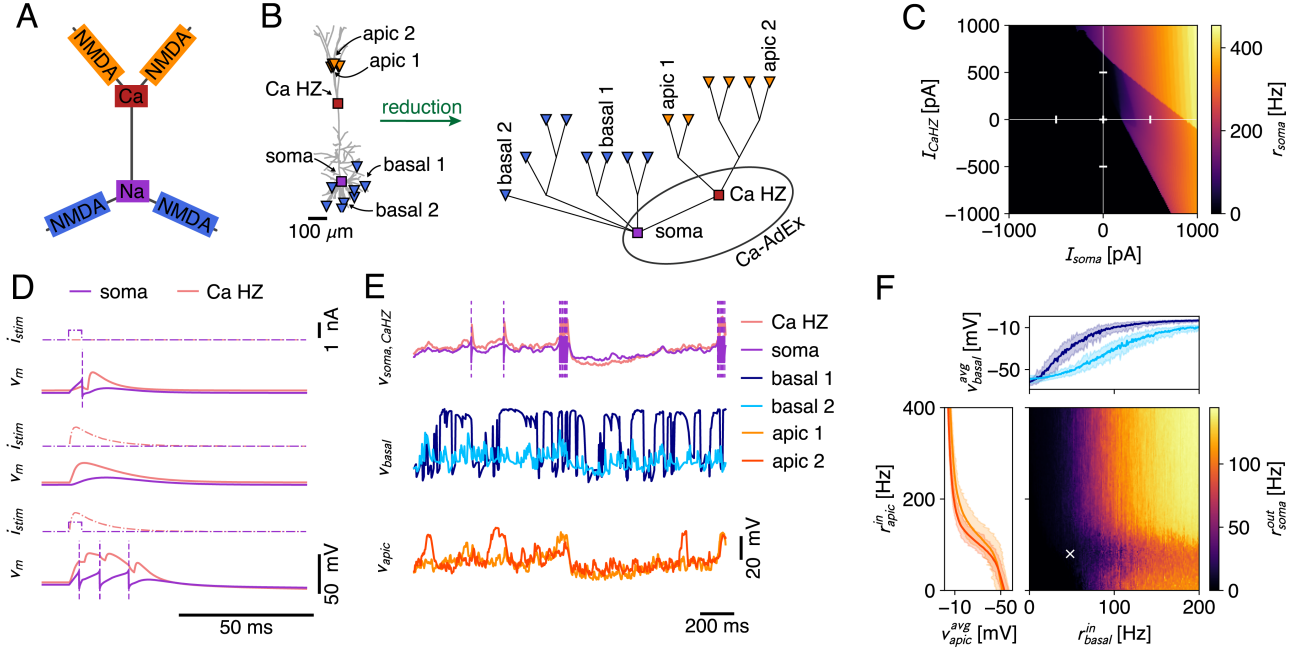


Figure 9: **A:** Canonical view of the interplay between dendritic non-linearities [28]. NMDA spikes in distal apical branches (orange) elicit Ca-spikes (red) that result in somatic burst firing (purple), whereas basal NMDA-spikes (blue) directly influence somatic output generation. **B:** Schematic of the creation process of the multicompart AdEx model. A passive morphology (left) with 16 locations (8 basal sites at $\sim 200 \mu\text{m}$ from the soma [blue triangles], 6 apical tuft sites at $\sim 1000 \mu\text{m}$ [orange triangles], the Ca-HZ where the apical trunk bifurcates [red square], and the soma [purple square]) is reduced to a simplified compartmental model (right) using the NEAT toolbox [66]. The Ca-hotzone and soma are then equipped with the Ca-spike generation mechanism and the AdEx mechanisms, respectively, where parameters were identical to the two compartment model. Labeled apical and basal sites are those for which traces and mean activations are shown in E and F. **C:** Firing rate response to input current steps that were applied to the soma and the Ca-hotzone compartment (same stimulation paradigm as in Figure 2-7). **D:** Simulation of the BAC-firing protocol, where a single output is generated in response to a somatic input pulse (top), no output is generated in response to a Ca-hotzone input (middle), and three output spikes are generated in response to the pairing of inputs (bottom). **E:** Exemplar traces for stimulation of the model with Poisson inputs that impinged on AMPA+NMDA synapses located at the basal and apical sites. Purple dashed lines indicate spike times. **F:** Firing rate response to increasing input rates to the apical and basal dendritic sites. Axes show the input rate to the individual dendritic sites (input rates were equal across apical resp. basal sites). Inset plots show the average membrane potential in two exemplar apical (left) and basal (top) compartments (same sites as in B, E). The min-max envelope shows the range of values obtained over all activation levels of the other area (i.e. apical vs basal). The white cross marks the input rates shown in E.

respectively equipped with the AdEx and Ca^{2+} -spike mechanisms, where we used the same parameters as the two-compartment model (Table 1). It speaks to the robustness of our approach that we achieve qualitatively similar behaviour as the two-compartmental model, without refitting any of the parameters (Figure 9C). Furthermore, this extended Ca-AdEx model also reproduced the BAC-firing protocol (Figure 9D). We then equip the apical (Figure 9B, orange) and basal (Figure 9B, blue) compartments with excitatory synapses containing both AMPA and NMDA receptor channels, as well as with an inhibitory GABAergic synapse. The latter was stimulated with a fixed Poisson rate of 20 Hz, whereas for the former we scanned a range of firing rates: for the apical synapses, we delivered Poisson rates between 0 and 400 Hz in 2 Hz increments, while for the basal synapses Poisson rates between 0 and 200 Hz were probed, in 1 Hz increments (Figure 9E,F). Simulations with each set of input rates were run for 2000 ms, and the average output rate was measured by averaging over five such episodes. The dendritic voltage traces exhibit signatures of the nonlinear dynamics associated with NMDA- and Ca^{2+} -channels (i.e. long up-states, burst firing, etc; Figure 9E). Furthermore, the averaged voltage responses in the apical and basal subunits follow the typical sigmoidal response curve [48, 34, 5, 44, 51] (Figure

9F, insets). These inset plots show the min-max envelope of the averaged voltage, i.e. for the apical voltage response (orange), the minimal values occurs for the lowest basal input level, whereas the maximal value occurs for the highest basal input level. That these min-max envelopes are close together and do not substantially affect the sigmoidal response curve, demonstrates that apical and basal areas are mutually independent [65]. Finally, the supralinear Ca^{2+} -spike mediated interaction between apical and basal areas is clearly visible in the output firing rates, where a strong increase occurs above a 100 Hz basal and a 100 Hz apical input rate (Figure 9F). We also remark that while the input and output rates seem high when considered as tonic firing rates, it is reasonable to assume that such rates can and do occur transiently, through the coincidence of multiple inputs to the apical and/or basal regions.

4 Discussion

Here we present the Ca-AdEx model, capturing the essential features of the apical-amplification, -isolation, and -drive regimes, at a modest computational cost compared to classical point-like neurons. This advancement supports the development of network models capable of emulating awake, NREM, and REM-like states, as well as the learning capabilities associated with the emergence of brain-state-specific bursting regimes in neurons that detect the coincidence of apical and somatic signals. Apical mechanisms play a crucial role in optimally combining internal priors and perceptual evidence within multi-areal hierarchical systems featuring lateral, top-down, and bottom-up connections. A significant observation is the drastic change in the firing rate of neurons where apical-amplification is active, which facilitates learning that aligns with the higher sampling rate of world experiences and is compatible with the STDP window of a few tens of milliseconds. Notably, an even more enhanced firing regime is associated with the apical-drive condition, potentially related to the replay and association of experiences during dreaming, whereas the suppression of the effect in apical-isolation supports the loss of consciousness during deeper sleep stages. Furthermore, as detailed in section 3.3, it is feasible to formulate, at a high level of abstraction, a compact geometric model capturing the effects produced by the combination of signals that convey information about priors and perceptual evidence, segregated into the apical and somatic compartments. The transfer function of the two-compartment Ca-AdEx model described here can be approximated piece-wise by low-order polynomials. Specifically, we examined the case of two approximating planes, giving rise to a class of transfer functions named $\text{ThetaPlanes}(I_s, I_d)$. ThetaPlanes represents a generalization for two-compartment neurons of the ReLU function commonly used to approximate single-compartment neuron models in numerous artificial intelligence algorithms. ThetaPlanes transfer functions can be implemented as efficient computational gates for use in large cognitive networks at a high level of abstraction. In future works, we plan to investigate the benefits of this computational gate in next-generation bio-inspired artificial intelligence algorithms. This expectation is supported by the emerging value of brain-state-specific bursting regimes demonstrated in recent works [9, 10]. These studies, while assuming the existence of such coincidence detection mechanisms as working hypotheses, lacked a biologically grounded transfer function.

Furthermore, the potential to maintain compatibility with the transfer function of widely adopted leaky integrate-and-fire models with adaptation when apical amplification is not triggered is promising. In our case, we aimed for compatibility with the Adaptive Exponential Integrate-and-Fire model (AdEx), which is extensively used for simulations at both micro- and meso-scales. It also serves as the basis for mean-field models for simulations encompassing the whole cortex [13]. We anticipate that during wakefulness, apical mechanisms and the sparsity of long-range connections will place a strict minority of neurons in a bursting regime. This adjustment is unlikely to significantly alter the average spectral signatures of expressed rhythms but could induce profound effects on perception and learning ability. Such a balance is necessary to maintain compatibility with the extensive body of experimental evidence concerning rhythms, average firing rates, and their fluctuations. During sleep, we anticipate that a delicate balance will be maintained to ensure healthy sleep patterns and to promote its beneficial cognitive and energetic effects. An additional noteworthy observation is that two-compartment neurons with significant transfer functions were efficiently discovered using the L2L framework within an evolutionary process that spanned only a hundred generations, each including no more than a hundred individuals. In our view, this suggests that natural evolution could have readily identified the cognitive advantages of apical mechanisms through localized variations of membrane and channel parameters, in ways somewhat analogous to the creation of two compartments. Thus, evolution might have incrementally given rise to the complex morphology seen in pyramidal neurons in the cortex.

Another aspect touched by our work is the role of high-performance computing (HPC) infrastructure, which offers a platform for conducting increasingly robust, comprehensive, and extensive explorations of parameter spaces

in scientific models. Coupled with machine learning, HPC emerges as a potent digital environment for adaptive testing and understanding the interactions between data and models. HPC allows scientists to simultaneously test a vast number of hypotheses within short time frames, delivering crucial information that can be incorporated into accelerated experimental cycles. Within this framework, L2L serves as an accessible tool for domain scientists to interface with HPC and conduct efficient parameter explorations. It allows focusing on areas of interest while offering a comprehensive overview of the entire parameter space, including the relationships between parameters and the selected fitness metrics. In this manuscript, we demonstrated that L2L is a framework adept at leveraging HPC infrastructure to assist neuroscientists in optimizing, fitting, and searching for suitable dynamics in models. Specifically, following the definition of the genome and the fitness functions for the multi-compartment neuron, an evolutionary algorithm can identify suitable candidates that survive the selection process. This work, based on a customization of the multi-compartment framework available in NEST [18, 54], also facilitates the inclusion of two- and many-compartment neuron models supporting apical mechanisms in the ecosystem of other standard simulation engines like Neuron [14] and Brian [55]. Additionally, this work outlines an approach grounded in traditional compartmental dynamics, which is computationally efficient and accurately captures the interplay between somatic action potentials (APs) and dendritic Ca^{2+} -spikes. As part of a broader compartmental modeling framework in NEST, our model can easily be expanded with additional compartments to represent other dendritic events, such as N-methyl-D-Aspartate (NMDA) spikes. Finally, due to its implementation in NEST, the model can be directly integrated into network simulations modeling incremental learning and sleep cycles.

5 Source code

[To be released on paper submission or by direct contact to start research partnership.](#)

6 Exemplary two-compartment Ca-AdEx neuron parameters

The evolutionary search detailed in the [Methods](#) Section identified an exemplary individual utilized throughout this paper unless specified otherwise (for instance, when discussing modulation to other brain states). Its complete genome is provided below. The parameters of the corresponding *ThetaPlanes* fitting function, as discussed in Section 2.6, are also reported below. [To be released on paper submission or by direct contact to start research partnership.](#)

7 Acknowledgments

This work has been co-funded by the European Next Generation EU grants CUP I53C22001400006 (FAIR PE0000013 PNRR Project) and CUP B51E22000150006 (EBRAINS-Italy IR00011 PNRR Project) and by the European Union Horizon 2020 Research and Innovation program under the FET Flagship Human Brain Project (grant agreement SGA3 n. 945539). Also, we acknowledge the usage of FENIX infrastructure computational resources under the ICEI project (grant agreement no. 800858) attributed to Chiara De Luca. In the end, we acknowledge the support of the APE Parallel/Distributed Computing Laboratory of INFN, Sezione di Roma. This research has also been partially funded by the Helmholtz Association through the Helmholtz Portfolio Theme Supercomputing and Modeling for the Human Brain.

8 Individual Contributions

- E.P. and P.S.P. Scientific conception, definition of neural activity equations and evolutionary fitness functions, definition of *ThetaPlanes* functions, analysis of results, initial manuscript writing.
- A.Y. and S.D. Learning to learn tool for evolutionary selection of optimal neural parameters, initial manuscript writing, support on HPC platforms.
- N.K. Fitting of *ThetaPlanes* functions, analysis of results, initial manuscript writing.
- W.W. Framework for multi-compartment neuron modeling in NEST, integration of Ca-AdEx in extended compartmental models, initial manuscript writing.

- F.S. Computational resources and system support.
- J.F.S. Definition of neural activity equations, biological plausibility of the multi-compartment neuron, initial manuscript writing

References

- [1] D. Aquilué-Llorens, J. S. Goldman, and A. Destexhe. “High-density exploration of activity states in a multi-area brain model”. In: *bioRxiv* (2023). DOI: 10.1101/2023.05.18.541285. eprint: <https://www.biorxiv.org/content/early/2023/05/18/2023.05.18.541285.full.pdf>. URL: <https://www.biorxiv.org/content/early/2023/05/18/2023.05.18.541285>.
- [2] J. Aru, F. Siclari, W. A. Phillips, and J. F. Storm. “Apical drive—A cellular mechanism of dreaming?”. In: *Neuroscience & Biobehavioral Reviews* 119 (2020), pp. 440–455.
- [3] J. Aru, M. Suzuki, and M. E. Larkum. “Cellular Mechanisms of Conscious Processing”. In: *Trends in cognitive sciences* 24.10 (Oct. 2020), pp. 814–825. ISSN: 1364-6613. DOI: 10.1016/j.tics.2020.07.006. URL: <https://doi.org/10.1016/j.tics.2020.07.006>.
- [4] B. F. Behabadi and B. W. Mel. “Mechanisms underlying subunit independence in pyramidal neuron dendrites.” In: *Proceedings of the National Academy of Sciences of the United States of America* 111.1 (Jan. 2014), pp. 498–503. ISSN: 1091-6490. DOI: 10.1073/pnas.1217645111. URL: <http://www.ncbi.nlm.nih.gov/pubmed/24357611> (visited on 01/22/2014).
- [5] T. Branco, B. Clark, and M. Hausser. “Dendritic discrimination of temporal input sequences in cortical neurons”. In: *Science Signalling* September (2010), pp. 1671–1675. DOI: 10.1126/science.1189664. URL: <http://stke.sciencemag.org/cgi/content/abstract/sci/329/5999/1671> (visited on 03/05/2013).
- [6] R. Brette and W. Gerstner. “Adaptive Exponential Integrate-and-Fire Model as an Effective Description of Neuronal Activity”. In: *Journal of Neurophysiology* 94.5 (2005). PMID: 16014787, pp. 3637–3642. DOI: 10.1152/jn.00686.2005. eprint: <https://doi.org/10.1152/jn.00686.2005>.
- [7] G. Buzsáki. “Hippocampal sharp wave-ripple: A cognitive biomarker for episodic memory and planning”. In: *Hippocampus* 25.10 (2015), pp. 1073–1188.
- [8] J. Cabral, M. L. Kringelbach, and G. Deco. “Functional connectivity dynamically evolves on multiple time-scales over a static structural connectome: Models and mechanisms”. In: *NeuroImage* 160 (2017), pp. 84–96. DOI: 10.1016/j.neuroimage.2017.03.045. URL: <http://dx.doi.org/10.1016/j.neuroimage.2017.03.045>.
- [9] C. Capone, C. Lupo, P. Muratore, and P. S. Paolucci. “Beyond spiking networks: The computational advantages of dendritic amplification and input segregation”. In: *PNAS* 120.49 (2023). ISSN: 1091-6490. DOI: 10.1073/pnas.2220743120. URL: <https://doi.org/10.1073/pnas.2220743120>.
- [10] C. Capone, C. Lupo, P. Muratore, and P. S. Paolucci. “Burst-Dependent Plasticity and Dendritic Amplification Support Target-Based Learning and Hierarchical Imitation Learning”. In: *Proceedings of Machine Learning Research* 162 (2022), pp. 2625–2637. URL: <https://proceedings.mlr.press/v162/capone22b.html>.
- [11] C. Capone, E. Pastorelli, B. Golosio, and P. S. Paolucci. “Sleep-like slow oscillations improve visual classification through synaptic homeostasis and memory association in a thalamo-cortical model”. In: *Scientific Reports* 9, 8990 (2019), pp. 1–11. ISSN: 2045-2322. DOI: 10.1038/s41598-019-45525-0. URL: <https://doi.org/10.1038/s41598-019-45525-0>.
- [12] C. Capone, B. Rebollo, A. Muñoz, X. Illa, P. Del Giudice, M. V. Sanchez-Vives, and M. Mattia. “Slow Waves in Cortical Slices: How Spontaneous Activity is Shaped by Laminar Structure”. In: *Cerebral Cortex* 29.1 (Nov. 2017), pp. 319–335. ISSN: 1047-3211. DOI: 10.1093/cercor/bhx326. eprint: <https://academic.oup.com/cercor/article-pdf/29/1/319/39386065/bhx326.pdf>. URL: <https://doi.org/10.1093/cercor/bhx326>.
- [13] C. Capone et al. “Simulations approaching data: cortical slow waves in inferred models of the whole hemisphere of mouse”. In: *Communications Biology* 6.266 (2023). DOI: 10.1038/s42003-023-04580-0. URL: <https://doi.org/10.1038/s42003-023-04580-0>.
- [14] N. T. Carnevale and M. L. Hines. “*The NEURON Book*”. Cambridge University Press, 2006. DOI: 10.1017/cbo9780511541612. URL: <https://doi.org/10.1017/cbo9780511541612>.
- [15] C. Clopath, R. Jolivet, A. Rauch, H.-R. Lüscher, and W. Gerstner. “Predicting neuronal activity with simple models of the threshold type: Adaptive Exponential Integrate-and-Fire model with two compartments”. In: *Neurocomputing* 70.10-12 (June 2007), pp. 1668–1673. ISSN: 09252312. DOI: 10.1016/j.neucom.2006.10.047. URL: <http://linkinghub.elsevier.com/retrieve/pii/S0925231206003602> (visited on 08/07/2012).
- [16] M. D’Andola, B. Rebollo, A. G. Casali, J. F. Weinert, A. Pigorini, R. Villa, M. Massimini, and M. V. Sanchez-Vives. “Bistability, Causality, and Complexity in Cortical Networks: An In Vitro Perturbational Study”. In: *Cerebral Cortex* 28.7 (May 2017), pp. 2233–2242. ISSN: 1047-3211. DOI: 10.1093/cercor/bhx122. eprint: <https://academic.oup.com/cercor/article-pdf/28/7/2233/40352561/bhx122.pdf>. URL: <https://doi.org/10.1093/cercor/bhx122>.
- [17] W. Gerstner, W. M. Kistler, R. Naud, and L. Paninski. “*Neuronal Dynamics: From Single Neurons to Networks and Models of Cognition*”. Cambridge University Press, 2014. DOI: 10.1017/CB09781107447615.
- [18] M.-O. Gewaltig and M. Diesmann. “NEST (NEural Simulation Tool)”. In: *Scholarpedia* 2.4 (2007), p. 1430. ISSN: 1941-6016. DOI: 10.4249/scholarpedia.1430.
- [19] B. Golosio, C. De Luca, C. Capone, E. Pastorelli, G. Stegel, G. Tiddia, G. De Bonis, and P. S. Paolucci. “Thalamo-cortical spiking model of incremental learning combining perception, context and NREM-sleep”. In: *PLoS Computational Biology* 17(6): e1009045 (2021), pp. 1–26. ISSN: 1553-7358. DOI: 10.1371/journal.pcbi.1009045. URL: <https://doi.org/10.1371/journal.pcbi.1009045>.
- [20] P. Hagmann, L. Cammoun, X. Gigandet, R. Meuli, C. J. Honey, J. Van Wassenhove, and O. Sporns. “The human connectome: A structural description of the human brain”. In: *PLoS Biology* 6(7): e159 (2008), pp. 1479–1493. DOI: 10.1371/journal.pbio.0060159. URL: <https://doi.org/10.1371/journal.pbio.0060159>.
- [21] E. Hay, S. Hill, F. Schürmann, H. Markram, and I. Segev. “Models of Neocortical Layer 5b Pyramidal Cells Capturing a Wide Range of Dendritic and Perisomatic Active Properties”. In: *PLoS Computational Biology* 7.7 (July 2011), pp. 1–18. DOI: 10.1371/journal.pcbi.1002107. URL: <https://doi.org/10.1371/journal.pcbi.1002107>.
- [22] M. Hines. “Efficient computation of branched nerve equations”. In: *International journal of bio-medical computing* 15.1 (1984), pp. 69–75. URL: <http://www.sciencedirect.com/science/article/pii/0020710184900084> (visited on 04/02/2013).
- [23] C. E. Jahr and C. F. Stevens. “Voltage Dependence of NMDA-Activated Macroscopic Conductances Predicted by Single-Channel Kinetics”. In: *The Journal of Neuroscience* 10.9 (1990), pp. 3178–3182. URL: <http://www.jneurosci.org/content/10/9/3178.short> (visited on 05/25/2013).

- [24] S. A. Josselyn, S. Köhler, and P. W. Frankland. “Finding the engram”. In: *Nature Review Neuroscience* 16 (2015), pp. 521–534. DOI: 10.1038/nrn4000. URL: <https://doi.org/10.1038/nrn4000>.
- [25] W. D. Killgore. “Effects of sleep deprivation on cognition”. In: *Progress in brain research* 185 (2010), pp. 105–129.
- [26] W. M. Kistler, W. Gerstner, and J. L. van Hemmen. “Reduction of the Hodgkin-Huxley equations to a single-variable threshold model”. In: *Neural Computation* 1045.1961 (1997), pp. 1015–1045. URL: <http://www.mitpressjournals.org/doi/abs/10.1162/neco.1997.9.5.1015> (visited on 04/03/2013).
- [27] M. Larkum. “A cellular mechanism for cortical associations: an organizing principle for the cerebral cortex”. In: *Trends in Neurosciences* 36.3 (2013), pp. 141–151. ISSN: 0166-2236. DOI: <https://doi.org/10.1016/j.tins.2012.11.006>. URL: <https://www.sciencedirect.com/science/article/pii/S0166223612002032>.
- [28] M. E. Larkum, T. Nevian, M. Sandler, A. Polsky, and J. Schiller. “Synaptic Integration in Tuft Dendrites of Layer 5 Pyramidal Neurons: A New Unifying Principle”. In: *Science* 325.5941 (Aug. 2009), pp. 756–760. ISSN: 0036-8075. DOI: 10.1126/science.1171958. URL: <http://www.sciencemag.org/cgi/doi/10.1126/science.1171958> (visited on 10/25/2012).
- [29] M. E. Larkum, W. Senn, and H.-R. Lüscher. “Top-down Dendritic Input Increases the Gain of Layer 5 Pyramidal Neurons”. In: *Cerebral Cortex* 14.10 (Oct. 2004), pp. 1059–1070. ISSN: 1047-3211. DOI: 10.1093/cercor/bhh065. eprint: <https://academic.oup.com/cercor/article-pdf/14/10/1059/771961/bhh065.pdf>. URL: <https://doi.org/10.1093/cercor/bhh065>.
- [30] M. E. Larkum, J. J. Zhu, and B. Sakmann. “A new cellular mechanism for coupling inputs arriving at different cortical layers.” In: *Nature* 398.6725 (Mar. 1999), pp. 338–341. ISSN: 1047-3211. DOI: 10.1038/18686.
- [31] C. D. Luca, L. Tonielli, E. Pastorelli, C. Capone, F. Simula, C. Lupo, I. Bernava, G. D. Bonis, G. Tiddia, B. Golosio, and P. S. Paolucci. “NREM and REM: cognitive and energetic gains in thalamo-cortical sleeping and awake spiking model”. In: *arXiv :2211.06889* (2023), pp. 1–22. DOI: 10.48550/arXiv.2211.06889. URL: <https://doi.org/10.48550/arXiv.2211.06889>.
- [32] J. F. MacDonald and J. M. Wojtowicz. “The effects of L-glutamate and its analogues upon the membrane conductance of central murine neurones in culture”. In: *Canadian Journal of Physiology and Pharmacology* 60.3 (1982). PMID: 6122493, pp. 282–296. DOI: 10.1139/y82-039. eprint: <https://doi.org/10.1139/y82-039>. URL: <https://doi.org/10.1139/y82-039>.
- [33] G. Major, M. E. Larkum, and J. Schiller. “Active properties of neocortical pyramidal neuron dendrites.” In: *Annual review of neuroscience* 36 (July 2013). ISBN: 0621111503, pp. 1–24. ISSN: 1545-4126. DOI: 10.1146/annurev-neuro-062111-150343. URL: <http://www.ncbi.nlm.nih.gov/pubmed/23841837> (visited on 07/02/2015).
- [34] G. Major, A. Polsky, W. Denk, J. Schiller, and D. W. Tank. “Spatiotemporally Graded NMDA Spike/Plateau Potentials in Basal Dendrites of Neocortical Pyramidal Neurons (Supplementary figures)”. In: *Journal of neurophysiology* (2008). URL: <http://jn.physiology.org/content/99/5/2584.short> (visited on 06/11/2015).
- [35] L. Muckli, F. D. Martino, L. Vizioli, L. S. Petro, F. W. Smith, K. Ugurbil, R. Goebel, and E. Yacoub. “Contextual Feedback to Superficial Layers of V1”. In: *Current Biology* 25.20 (2015), pp. 2690–2695. ISSN: 0960-9822. DOI: <https://doi.org/10.1016/j.cub.2015.08.057>. URL: <https://www.sciencedirect.com/science/article/pii/S0960982215010738>.
- [36] R. Naud, B. Bathellier, and W. Gerstner. “Spike-timing prediction in cortical neurons with active dendrites.” In: *Frontiers in computational neuroscience* 8.August (Jan. 2014), p. 90. ISSN: 1662-5188. DOI: 10.3389/fncom.2014.00090. URL: <http://www.pubmedcentral.nih.gov/articlerender.fcgi?artid=4131408&tool=pmcentrez&rendertype=abstract> (visited on 08/18/2015).
- [37] C. Nowke, S. Diaz-Pier, B. Weyers, B. Hentschel, A. Morrison, T. W. Kuhlen, and A. Peyser. “Toward rigorous parameterization of underconstrained neural network models through interactive visualization and steering of connectivity generation”. In: *Frontiers in neuroinformatics* 12 (2018), p. 32.
- [38] M. Pagkalos, S. Chavlis, and P. Poirazi. “Introducing the Dendrixy framework for incorporating dendrites to spiking neural networks”. In: *Nature Communications* 14.1 (Jan. 2023), p. 131. ISSN: 2041-1723. DOI: 10.1038/s41467-022-35747-8. URL: <https://www.nature.com/articles/s41467-022-35747-8> (visited on 09/15/2023).
- [39] P. Papale, F. Wang, A. T. Morgan, X. Chen, A. Gilhuis, L. S. Petro, L. Muckli, P. R. Roelfsema, and M. W. Self. “The representation of occluded image regions in area V1 of monkeys and humans”. In: *Current Biology* 33.18 (2023), 3865–3871.e3. ISSN: 0960-9822. DOI: <https://doi.org/10.1016/j.cub.2023.08.010>. URL: <https://www.sciencedirect.com/science/article/pii/S0960982223010539>.
- [40] E. Pastorelli, C. Capone, F. Simula, M. V. Sanchez-Vives, P. Del Giudice, M. Mattia, and P. S. Paolucci. “Scaling of a Large-Scale Simulation of Synchronous Slow-Wave and Asynchronous Awake-Like Activity of a Cortical Model With Long-Range Interconnections”. In: *Frontiers in Systems Neuroscience* 13 (2019). ISSN: 1662-5137. DOI: 10.3389/fnsys.2019.00033. URL: <https://www.frontiersin.org/articles/10.3389/fnsys.2019.00033>.
- [41] W. A. Phillips, M. E. Larkum, C. W. Harley, and S. M. Silverstein. “The effects of arousal on apical amplification and conscious state”. In: *Neuroscience of Consciousness* 2016.1 (Sept. 2016), niw015. ISSN: 2057-2107. DOI: 10.1093/nc/niw015. eprint: <https://academic.oup.com/nc/article-pdf/2016/1/niw015/25445653/niw015.pdf>. URL: <https://doi.org/10.1093/nc/niw015>.
- [42] W. A. Phillips. *The Cooperative Neuron: Cellular Foundations of Mental Life*. Oxford University Press, Apr. 2023. ISBN: 9780198876984. DOI: 10.1093/oso/9780198876984.001.0001. URL: <https://doi.org/10.1093/oso/9780198876984.001.0001>.
- [43] P. F. Pinsky and J. Rinzel. “Intrinsic and network rhythmogenesis in a reduced traub model for CA3 neurons”. In: *Journal of Computational Neuroscience* 1.1-2 (1994). ISBN: 0929-5313 (Print), pp. 39–60. ISSN: 09295313. DOI: 10.1007/BF00962717.
- [44] P. Poirazi, T. Brannon, and B. W. Mel. “Arithmetic of subthreshold synaptic summation in a model CA1 pyramidal cell”. In: *Neuron* 37.6 (2003), pp. 977–987. URL: <http://www.sciencedirect.com/science/article/pii/S089662730300148X> (visited on 04/02/2013).
- [45] C. Pozzorini, S. Mensi, O. Hagens, R. Naud, C. Koch, and W. Gerstner. “Automated High-Throughput Characterization of Single Neurons by Means of Simplified Spiking Models.” In: *PLoS computational biology* 11.6 (June 2015), e1004275. ISSN: 1553-7358. DOI: 10.1371/journal.pcbi.1004275. URL: <http://www.ncbi.nlm.nih.gov/pubmed/26083597> (visited on 06/23/2015).
- [46] P. Rhodes. “The properties and implications of NMDA spikes in neocortical pyramidal cells.” In: *The Journal of neuroscience : the official journal of the Society for Neuroscience* 26.25 (June 2006), pp. 6704–15. ISSN: 1529-2401. DOI: 10.1523/JNEUROSCI.3791-05.2006. URL: <http://www.ncbi.nlm.nih.gov/pubmed/16793878> (visited on 06/11/2015).
- [47] S. Rotter and M. Diesmann. “Exact digital simulation of time-invariant linear systems with applications to neuronal modeling.” In: *Biological cybernetics* 81.5-6 (Nov. 1999), pp. 381–402. ISSN: 0340-1200. URL: <http://www.ncbi.nlm.nih.gov/pubmed/10592015>.
- [48] J. Schiller, G. Major, H. Koester, and Y. Schiller. “NMDA spikes in basal dendrites of cortical pyramidal neurons”. In: *Nature* 404.6866 (2000), pp. 285–289. URL: <http://www.nature.com/nature/journal/v404/n6775/abs/404285a0.html> (visited on 06/02/2015).
- [49] I. Segev. “Untangling Dendrites with Quantitative Models”. In: *Science* 290.5492 (Oct. 2000), pp. 744–750. ISSN: 00368075. DOI: 10.1126/science.290.5492.744. URL: <http://www.sciencemag.org/cgi/doi/10.1126/science.290.5492.744> (visited on 04/09/2013).
- [50] T. J. Sejnowski and A. Destexhe. “Why do we sleep?” In: *Brain research* 886.1-2 (2000), pp. 208–223.

- [51] M. F. Singh and D. H. Zald. “A simple transfer function for nonlinear dendritic integration.” In: *Frontiers in computational neuroscience* 9.August (Jan. 2015), p. 98. ISSN: 1662-5188. DOI: 10.3389/fncom.2015.00098. URL: <http://www.pubmedcentral.nih.gov/articlerender.fcgi?artid=4530314&tool=pmcentrez&rendertype=abstract> (visited on 02/01/2016).
- [52] “SleepEnhancesPlasticity intheDevelopingVisualCortex”. In: *Neuron* 30 (2001), pp. 275–287. DOI: 10.1016/S0896-6273(01)00279-3. URL: [https://doi.org/10.1016/S0896-6273\(01\)00279-3](https://doi.org/10.1016/S0896-6273(01)00279-3).
- [53] O. Sporns, G. Tononi, and R. Kötter. “The human connectome: A structural description of the human brain”. In: *PLoS Computational Biology* 1(4):e42 (2005), pp. 245–251. DOI: 10.1371/journal.pcbi.0010042. URL: <https://doi.org/10.1371/journal.pcbi.0010042>.
- [54] S. Spreizer et al. *NEST 3.3*. Version 3.3. Mar. 2022. DOI: 10.5281/zenodo.6368024. URL: <https://doi.org/10.5281/zenodo.6368024>.
- [55] M. Stimberg, R. Brette, and D. F. Goodman. “Brian 2, an intuitive and efficient neural simulator”. In: *eLife* 8 (Aug. 2019). Ed. by F. K. Skinner, e47314. ISSN: 2050-084X. DOI: 10.7554/eLife.47314.
- [56] M. Suzuki and M. E. Larkum. “General Anesthesia Decouples Cortical Pyramidal Neurons”. In: *Cell* 180.4 (2020), 666–676.e13. ISSN: 0092-8674. DOI: <https://doi.org/10.1016/j.cell.2020.01.024>. URL: <https://www.sciencedirect.com/science/article/pii/S0092867420301057>.
- [57] S. Thrun and L. Pratt. “*Learning to learn*”. Springer Science & Business Media, 2012.
- [58] S. Thrun and L. Pratt. “Learning to learn: Introduction and overview”. In: *Learning to learn*. Springer, 1998, pp. 3–17.
- [59] G. Tononi and C. Cirelli. “Sleep and synaptic down-selection”. In: *European Journal of Neuroscience* 51.1 (2020), pp. 413–421. DOI: 10.1111/ejn.14335. eprint: <https://onlinelibrary.wiley.com/doi/pdf/10.1111/ejn.14335>. URL: <https://onlinelibrary.wiley.com/doi/abs/10.1111/ejn.14335>.
- [60] G. Tononi and C. Cirelli. “Sleep and the price of plasticity: From synaptic and cellular homeostasis to memory consolidation and integration”. In: *Neuron* 81 (2014), pp. 12–34. ISSN: 0896-6273. DOI: 10.1016/j.neuron.2013.12.025. URL: <https://doi.org/10.1016/j.neuron.2013.12.025>.
- [61] M. di Volo, A. Romagnoni, C. Capone, and A. Destexhe. “Biologically Realistic Mean-Field Models of Conductance-Based Networks of Spiking Neurons with Adaptation”. In: *Neural Computation* 31.4 (Apr. 2019), pp. 653–680. ISSN: 0899-7667. DOI: 10.1162/neco_a_01173. URL: https://doi.org/10.1162/neco_a_01173.
- [62] B. O. Watson, D. Levenstein, J. P. Greene, J. N. Gelinis, and G. Buzsáki. “Network Homeostasis and State Dynamics of Neocortical Sleep”. In: *Neuron* 90.4 (2016), pp. 839–852. ISSN: 0896-6273. DOI: <https://doi.org/10.1016/j.neuron.2016.03.036>. URL: <http://www.sciencedirect.com/science/article/pii/S0896627316300563>.
- [63] W. A. M. Wybo, D. Boccalini, B. Torben-Nielsen, and M.-O. Gewaltig. “A Sparse Reformulation of the Green’s Function Formalism Allows Efficient Simulations of Morphological Neuron Models.” In: *Neural computation* 27.12 (Dec. 2015), pp. 2587–622. ISSN: 1530-888X. DOI: 10.1162/NECO_a_00788. URL: <http://www.ncbi.nlm.nih.gov/pubmed/26496043>.
- [64] W. A. M. Wybo, K. M. Stiefel, and B. Torben-Nielsen. “The Green’s function formalism as a bridge between single- and multi-compartmental modeling.” In: *Biological cybernetics* 107.6 (Sept. 2013), pp. 685–694. ISSN: 1432-0770. DOI: 10.1007/s00422-013-0568-0. URL: <http://www.ncbi.nlm.nih.gov/pubmed/24037222> (visited on 09/17/2013).
- [65] W. A. Wybo, B. Torben-Nielsen, T. Nevian, and M. O. Gewaltig. “Electrical Compartmentalization in Neurons”. In: *Cell Reports* 26.7 (2019). Publisher: ElsevierCompany., 1759–1773.e7. ISSN: 22111247. DOI: 10.1016/j.celrep.2019.01.074. URL: <https://doi.org/10.1016/j.celrep.2019.01.074>.
- [66] W. A. Wybo, J. Jordan, B. Ellenberger, U. Marti Mengual, T. Nevian, and W. Senn. “Data-driven reduction of dendritic morphologies with preserved dendro-somatic responses”. In: *eLife* 10 (Jan. 2021). Ed. by T. O’Leary, R. L. Calabrese, H. P. Robinson, and M. F. Nolan. Publisher: eLife Sciences Publications, Ltd, e60936. ISSN: 2050-084X. DOI: 10.7554/eLife.60936. URL: <https://doi.org/10.7554/eLife.60936> (visited on 07/20/2022).
- [67] A. Yegenoglu, K. Krajsek, S. D. Pier, and M. Herty. “Ensemble kalman filter optimizing deep neural networks: an alternative approach to non-performing gradient descent”. In: *Machine Learning, Optimization, and Data Science: 6th International Conference, LOD 2020, Siena, Italy, July 19–23, 2020, Revised Selected Papers, Part II* 6. Springer. 2020, pp. 78–92.
- [68] A. Yegenoglu, A. Subramoney, T. Hater, C. Jimenez-Romero, W. Klijn, A. P. Martín, M. van der Vlag, M. Herty, A. Morrison, and S. Díaz-Pier. “Exploring Parameter and Hyper-Parameter Spaces of Neuroscience Models on High Performance Computers With Learning to Learn”. In: *Frontiers in Computational Neuroscience* 16 (2022). DOI: [doi:10.3389/fncom.2022.885207](https://doi.org/10.3389/fncom.2022.885207).